Spring 2017

A Quantum Astrochemical Perspective on the c-C3H Radical with Application to the Interstellar Medium

Matthew Bassett

A QUANTUM ASTROCHEMICAL PERSPECTIVE ON THE c-C_3H RADICAL WITH APPLICATION TO THE INTERSTELLAR MEDIUM

by

MATTHEW BASSETT

(Under the Direction of Ryan Fortenberry)

ABSTRACT

The interstellar medium (ISM) has been an area of focus for astrochemists and quantum chemists for many years, with particular interest in the presence of interstellar molecules and the resulting chemical processes. The c-C_3H radical has been detected in the ISM near the dark molecular cloud TMC-1. With the application of $ab\ initio$ computational methods using coupled-cluster theory at the singles, doubles, and perturbative triples [CCSD(T)] level, highly accurate quartic force fields (QFFs) are constructed to define the electronic wavefunction for the inter nuclear Hamiltonian. The QFF is used to predict the equilibrium geometry and produce vibrational frequencies, rotational constants, and other spectroscopic data. Moreover, the data produced can be used for corroboration of experiment or previous theory as well as potential detection in the ISM.

INDEX WORDS : Theoretical chemistry, Quantum chemistry, Astrochemistry, Polycyclic aromatic hydrocarbons, Quartic force fields, Coupled-cluster theory, Interstellar molecules, Interstellar medium, Interstellar chemistry.

A QUANTUM ASTROCHEMICAL PERSPECTIVE ON THE c-C_3H RADICAL WITH APPLICATION TO THE INTERSTELLAR MEDIUM

by

MATTHEW BASSETT

B.S., Georgia Southern University, 2015

A Thesis Submitted to the Graduate Faculty of Georgia Southern University in Partial Fullfillment of the Requirements for the Degree

MASTER OF SCIENCE

STATESBORO, GEORGIA

A QUANTUM ASTROCHEMICAL PERSPECTIVE ON THE c-C_3H RADICAL WITH APPLICATION TO THE INTERSTELLAR MEDIUM

by

MATTHEW BASSETT

Major Professor: Ryan Fortenberry

Committee: Ji Wu

Mark Edwards

Electronic Version Approved

May 2017

I wish to extend my gratitude to Georgia Southern University (GSU) for resources and funding provided for me to conduct research. Particularly, I would like to thank the Student Government Association for providing travel funding and resources to present my research to other astrochemists along with the rest of the scientific c ommunity. I would also like to thank Department of Chemistry and Biochemistry at GSU for giving me the opportunity to conduct research for a Master of Sciences degree in Applied Physical Sciences with emphasis in Chemistry. Last, but certainly not least, I would like to thank Dr. Ryan Fortenberry for taking me on as a graduate assistant and teaching me the ever necessary skills for continuing my research, with the occasional life lesson. Thank you to all who have supported me in my endeavors both academically and personally.

TABLE OF CONTENTS

LIST OF FIGURES

LIST OF TABLES

Chapter 1

Introduction

1.1 Astrochemistry

Theoretical and experimental astrochemists have been turning their efforts towards the heavens to further our understanding of interstellar molecular species and the chemical reactions they may undergo in the interstellar medium (ISM) since the early part of the 20^{th} century. These molecular species are the product of stellar chemistry and are dispersed through the ISM via supernova and stellar winds and are commonly found in dark molecular clouds and circumstellar envelopes. A couple of the most common regions observed by astrochemists are the Taurus Molecular Cloud (TMC-1) and the circumstellar envelope around IRC +10216[2,3]. A catalog of known interstellar molecules[4,5] has been amassed along with a list of their relative abundances throughout the ISM[6,7].

The chaotic physical characteristics of these regions in the ISM allows the formation of molecules that are too unstable to exist on Earth, such as radicals. The low pressures and temperatures of diffuse space allow the extremely reactive unpaired electron to exist due to a lower potential to collide with other molecules, whereas the higher pressures and temperatures of Earth are unsupportive for the existence of molecular radicals.

The formation of interstellar radicals has been attributed to the high reactivity of carbon chains, and in some cases, are suggested to be the precursors for the creation of interstellar anions. Moreover, interstellar radicals have long been hypothesized to be the crucial link to the formation of polycyclic aromatic hydrocarbons (PAHs)[8,9]. The interstellar chemistry associated with potential PAHs has been widely studied across the field of theoretical astrochemistry and astrophysics. Nearly all PAH species have transitions in the infrared (IR) and near-IR region. Quantum chemical methods have allowed for definition of the IR emissions of various PAHs previously documented[10]. A database of cataloged interstellar molecules, including PAHs, is available through the Astrochemistry Laboratory at NASA Ames Research Center. This database, relies heavily upon the use of quantum chemistry to maintain current and accurate knowledge of the molecular species that exist or are yet to be detected; experiment can only provide some understanding. Moreover, theoretical approaches have been successful in processing large amounts of throughput to provide highly detailed data such as vibrational frequencies, intensities, and relative energies, which are used for labeling previously unattributed lines in observed spectra[11]. It is in this light, the work presented here seeks to add to the understanding of the chemical composition and subsequent interactions throughout interstellar and circumstellar regions of space[12].

The mystery of it all is derived from the spectral lines that are unattributed to any known interstellar molecules. However, this mystery has opened the door for more powerful telescopes for less noisy spectra and the application of quantum chemical methods to predict these unknown bands. As astronomical spectroscopy has progressed as a discipline, it has become easier to identify lines in interstellar spectra with the help of experiment and quantum chemical techniques[11].

1.2 Spectroscopy

Spectroscopy, the study of the interaction of light with matter, is used on the astronomical scale to observe spectra of various regions throughout the universe. The process is used to determine the energy given off when a photon of light, otherwise known as electromagnetic radiation, comes into contact with matter. The energy, E, is measured by a function of the speed of light, c, over the wavelength of the photon, λ, also called the frequency, ν, and multiplied by Planck's constant, h. Thus, energy is defined as[13]:

$$E = \frac{hc}{\lambda} = h\nu. \tag{1.1}$$

While observed data are crucial to identification and characterization of interstellar molecules, quantum theory has been paramount in gaining a more accurate picture of the interstellar species that exist within molecular clouds and circumstellar envelopes. When molecules absorb this en-

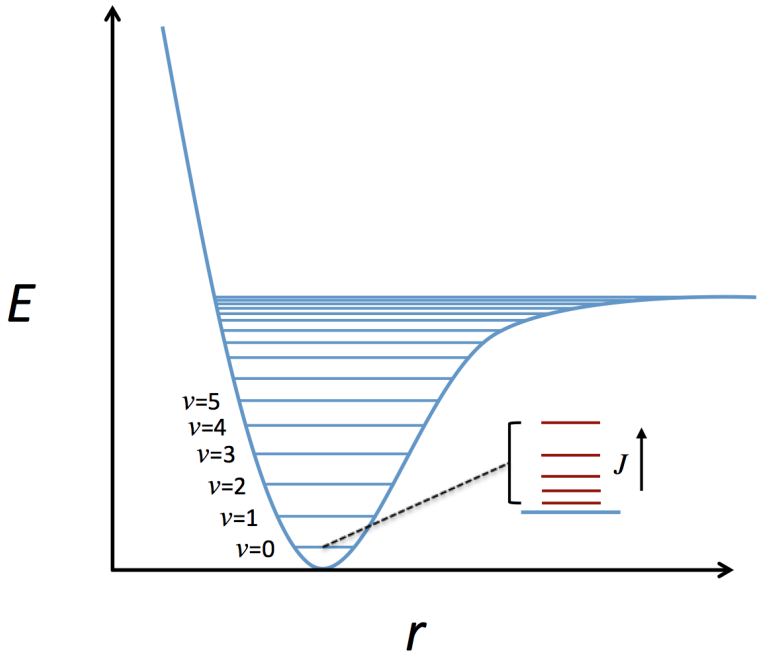

Figure 1.1: Ideal rovibrational energy levels of a diatomic molecule [1]

ergy, the interaction is varied based on the wavelength of the photon and the molecular structure. Spectroscopic instruments detect the wavelength of light being emitted by the interacting molecule and its intensity. Photons of lower energy play an integral role in describing the rotations and vibrations of molecules via quantized energy levels. The energies are plotted as a quasi-morse potential energy surface (PES) [14,15] as shown in Figure 1.1, where the vibrational and rotational excitation levels within the single electronic state are notated as ν_n and J respectively.

The vibrations of the molecule arise from each molecule's specific set of internal dynamics, or normal coordinates, which define its electronic structure. These are dynamics are represented in the various motions within bond stretching, bending, and torsions. The corresponding vibrational frequencies are observed through infrared spectroscopy; while radio, millimeter, and microwave spectroscopy is required for observing the rotational excitations. The difficulty lies in distinguishing the hyperfine rotational sub-structure[16–18] within the vibrational transitions. Therefore, the overall molecular structure can be inferred from the shape of the features in the spectra[19,20]. This is where quantum chemical theory is most useful in defining the PES and subsequent rovibrational spectra for specific molecules without the added noise of surrounding matter. The computed hyperfine structure can be confirmed by matching the rotational and vibrational transitions from theoretical spectra with that of the observed spectra.

However, the quantum chemical methods require highly-accurate spectroscopic constants to be of any use for proper characterization. As molecular complexity and size increase, the difficulty of fully defining a given transition increases, as well as the presence of any potential coupling[18] through Coriolis[21], Fermi[22], and Darling-Dennison resonances[23].

The methods of spectroscopy have evolved significantly over the past century, where modern spectroscopy has been able to detect lines at the rotational level, thus revealing intensity peaks that were previously perceived as noise. One such telescope exists in the Chiléan desert, the Atacama Large Millimeter Array (ALMA)[24,25]. While other telescopes, like the Stratospheric Observatory for Infrared Astronomy (SOFIA)[26,27], have been instrumental in the detection of previously unknown interstellar molecules, ALMA can provide higher resolution for spectra than any prior

spectroscopic telescopes. The future, however, will rely on data generated by quantum chemical methods for characterization and detection of new molecular species[28]. The use of high-level rovibrational computations has been successful in producing rotational constants within 15 MHz and vibrational frequencies within 1.0 cm^{-1} of experiment[28–37]. Furthermore, these methods can produce observed spectra of the various frequencies which are used in identifying specific molecular species, in this case, throughout the universe.

1.3 Theoretical Chemistry

1.3.1 Electronic Structure

The electronic molecular structure is defined by the molecular function, or wavefunction. The ground electronic state, or the lowest energy state, of a given molecule will be the most populated state. The electronic structure can be solved under the time-independent non-relativistic Schrödinger equation[38] represented as,

$$\hat{H}\Psi = E\Psi. \tag{1.2}$$

The Hamiltonian, $\hat{H}$, is an operator that treats the wavefunction, Ψ, as an eigenfunction, which produces the energy while continually returning the starting wavefunction. The molecular

Hamiltonian can be expressed as a sum of its kinetic $\hat{T}$ and potential $\hat{V}$ pieces, which is defined as,

$$\hat{H} = -\sum_{i=1}^{N}\frac{1}{2}\nabla_i^2 - \sum_{A=1}^{M}\frac{1}{2M_A}\nabla_A^2 - \sum_{i=1}^{N}\sum_{A=1}^{M}\frac{Z_A}{r_{iA}} + \sum_{i=1}^{N}\sum_{j=1}^{M}\frac{1}{r_{ij}} + \sum_{A=1}^{N}\sum_{B=1}^{M}\frac{Z_A Z_B}{R_{AB}}, \tag{1.3}$$

where N and ij are indices for the total number and individual electrons accordingly; while M and AB are the indices for the total number and individual nuclei respectively. All variables are represented in atomic units. Each piece of the molecular Hamiltonian represents a specific motion for interaction of electrons and nuclei. Thus, the molecular Hamiltonian can be simplified to the more common definition written as,

$$\hat{H} = \hat{T}_e + \hat{T}_N + \hat{V}_{eN} + \hat{V}_{ee} + \hat{V}_{NN}, \tag{1.4}$$

where ($\hat{T}_e$) is the kinetic energy of electron motion, ($\hat{T}_N$) is the nuclear motion, ($\hat{V}_{eN}$) is the nuclear-electronic attraction, ($\hat{V}_{ee}$) is the electronic repulsion, and ($\hat{V}_{NN}$) is the nuclear repulsion.

Under the Born-Oppenheimer (BO) approximation, the nuclei of the molecule are assumed to be fixed points in space, therefore the kinetic energy of nuclear motion ($\hat{T}_N$) is reduced to be zero and the potential energy of the nuclear-nuclear repulsion ($\hat{V}_{NN}$) is constant[39]. The new Hamiltonian under the constraint of the BO approximation is reduced to its electronic components[40]. The electronic Hamiltonian is expressed as,

$$\hat{H}_{elec} = \hat{T}_e + \hat{V}_{eN} + \hat{V}_{ee}. \tag{1.5}$$

which is an easier problem for quantum chemical methods to solve for the molecular wavefunction.

The most common methods for constructing the wavefunction use Hartree-Fock (HF) or the Self-Consistent Field (SCF) theory to optimize the formation and occupation of molecular orbitals (MO) by minimizing the molecular energy through the variational principle[41–44]. The SCF approach uses a linear combination of atomic orbitals to create molecular orbitals (LCAO-MO) in an even tempered fashion[45–48]. Under the LCAO-MO method, a single spatial orbital is assumed to be occupied by two spin-opposite electrons. Alternatively, basis functions can be spin orbitals. Both can be represented as a Slater determinant[49], with spatial orbitals requiring fewer computational resources.

The SCF method yields a single variationally-optimized Slater determinant, which is assumed represent the ground electronic state of a given molecular species. This computation produces a starting guess for most molecules. Yet, the electron-electron repulsion operator, $\hat{V}_{ee}$, remains as the limiting factor for high accuracy and cost efficacy. SCF theory does not explicitly treat the electron-electron correlation but treats the location of a single electron in relation to the remaining electron field. However, theories have been developed to explicitly treat electron correlation for the solution of $\hat{V}_{ee}$. These methods compute the contribution from determinants by allowing unoccupied virtual orbitals to be accessed by electrons from the occupied orbitals of the ground state. The definition of the wavefunction is paramount for producing the most accurate data with efficient use of time. The restricted Hartree-Fock (RHF) method only treats explicitly closed-shell molecules, which means only pairs of electrons. RHF methods are fast and cheap, but with a lower chance for high accuracy[50]. Alternatively, the unrestricted Hartree-Fock (UHF) method can treat individual

electrons which is useful for both closed-shell and open-shell molecules. UHF methods are less accurate and significantly more costly[51,52]. In an effort to find a middle ground, the restricted open-shell Hartree-Fock (ROHF) method was developed as a way to treat all paired and unpaired electrons as well as all possible combinations in an efficient manner[53].

1.3.2 Coupled Cluster Theory

It has long been thought that the most powerful and robust methods in quantum chemistry for treating dynamic electron correlation effects are based on the coupled-cluster (CC) approximation[54,55]. The goal with CC methods is to approximate the full configuration interaction (FCI) of electron correlation[56,57]. This non-variational CC method of treating electron correlation is more complete than other linear methods at a given truncation level. The most simplified form of the CC wavefunction is expressed as[58],

$$|\Psi_{CC}\rangle = e^{\hat{T}}|\Phi_0\rangle \tag{1.6}$$

where Φ_0 is the reference wavefunction[58] and $\hat{T}$ is the cluster operator.

The reference wavefunction, Φ_0, is the HF single Slater determinant; and the cluster operator, $\hat{T}$, can be expressed as a power-series expansion of the linear excitation operator truncated at the chosen level of excitation. The resulting CC wavefunction is written as,

$$|\Psi_{CC}\rangle = (1 + \hat{T} + \frac{1}{2!}\hat{T}^2 + \frac{1}{3!}\hat{T}^3 + ...)|\Phi_0\rangle \tag{1.7}$$

and $\hat{T}$ can be expressed as,

$$\hat{T} = \hat{T}_1 + \hat{T}_2 + \hat{T}_3 + ... \,. \tag{1.8}$$

The singles excitation is $\hat{T}_1$, doubles is $\hat{T}_2$, triples is $\hat{T}_3$.

The coupled-cluster singles and doubles (CCSD) method is often not efficient enough to produce the desired accuracy for its applications[55,59]. The full CCSDT method has shown to be sufficient in producing high quality and highly accurate data with the drawback of being significantly more costly, thus more restricted from use in computational chemistry[55,60–62]. A noniterative approach to approximate the triples contribution has been widely used as a cheaper way of achieving near CCSDT quality results. The resulting method is CCSD with a perturbative triples calculation to form CCSD(T)[55]. The CCSD(T) electronic wavefunction is defined as[56–58,63];

$$E_{CCSD(T)} = E_{CCSD} + E_T. \tag{1.9}$$

1.3.3 Quartic Force Fields

The internuclear Hamiltonian is defined as,

$$H = \frac{1}{2}\sum_{\rho\sigma}(J_\rho - \pi_\rho)\mu_{\rho\sigma}(J_\sigma - \pi_\sigma) - \frac{1}{2}\sum_k \frac{\delta^2}{\delta Q_k^2} - \frac{1}{8}\sum_\rho \mu_{\rho\rho} + V(Q) \tag{1.10}$$

where J_ρ is the total angular momentum of a given cartesian direction (x, y, or z) notated as ρ and

σ; π_ρ is the total vibrational angular momentum in the same direction; $\mu_{\rho\sigma}$ is the inverse of the momentum of inertia tensor; and Q is the set of all normal coordinates[64].

Quartic force fields (QFFs) are used to accurately define the potential energy surfaces (PESs) for the anharmonic nuclear potential[65–67]. QFFs are a fourth-order Taylor series expansion approximations to the potential of the internuclear Hamiltonian and are defined as,

$$V = \frac{1}{2}\sum_{ij} F_{ij}\Delta_i\Delta_j + \frac{1}{6}\sum_{ijk} F_{ijk}\Delta_i\Delta_j\Delta_k + \frac{1}{24}\sum_{ijkl} F_{ijkl}\Delta_i\Delta_j\Delta_k\Delta_l \tag{1.11}$$

with force constants in terms of $F_{ij...}$ and displacements of Δ_i[29,68–70].

Often enough, CC methods that employ the QFF approach produces results with accuracies within 5% , and often within 1% , of experimental fundamental vibrational frequencies for a variety of methods[29–31,68–78]. However, the QFFs that produce the most accurate electronic structures are used under the CCSD(T) method[55,79].

A composite CBS extrapolated core correlation relativistic (CcCR) reference geometry is calculated by using CCSD(T)-based QFFs with various basis sets. The augmented correlation consistent aug-cc-pV5Z basis set is used to compute the starting geometry[80,81]. A correction to core-correlation effects are made by adding the difference between a calculation using the Martin-Taylor (MT) basis set with, MTc, and without, MT, the contribution of core electrons[82]. The CcCR reference geometry is defined as,

$$R = R_{5Z} + (R_{MTc} - R_{MT}). \tag{1.12}$$

with R representing some geometrical component[66].

From the CcCR reference geometry a grid of symmetry-unique points are generated based on a set of molecule specific symmetry-internal coordinates. At each point on the QFF a CCSD(T) energy calculation is performed at the aug-cc-pVXZ basis sets, where X is T, Q, or 5, hereby noted as TZ, QZ, or 5Z respectively[80,81,83]. These calculations are extrapolated to the complete basis set (CBS) limit[84]. The resulting QFF is then corrected for core-correlation effects by calculations using the MTc and MT basis sets[82]. Subsequently, the QFF is further corrected for scalar relativistic correction by the adding the difference between calculations using the Douglas-Kroll (DK) basis sets with, DKr, and without, DK, scalar relativistic contributions[85]. The subsequent CcCR QFF composite energy scheme is defined as[67],

$$E_{CcCR} = E_{CBS} + (E_{MTc} - E_{MT}) + (E_{apVTZ-DKr} - E_{apVTZ-DK}). \tag{1.13}$$

In a similar fashion, a CcCE reference geometry is computed for benchmark comparisons to the CcCR produced results. A starting CCSD/5Z geometry is computed and corrected for core-correlation effects using the MTc and MT basis sets at the CCSD level. Since CCSD does not have a triples calculation, an additive triples correction is made by subtracting a calculation made at the CCSD/TZ level and basis set from that of the CC3/TZ level and basis[66,71,86]. The CcCE reference geometry is constructed as follows,

$$R = R_{5Z} + (R_{MTc} - R_{MT}) + (R_{CC3/TZ} - R_{CCSD/TZ}). \tag{1.14}$$

As it should follow, the CcCE QFF is constructed similarly to the CcCR QFF. However, the relativistic corrections are eliminated and replaced with a correlated triples correction calculation at the CC3/TZ level and basis. The resulting CcCE QFF is defined as[67],

$$E_{CcCE} = E_{CBS} + (E_{MTc} - E_{MT}) + (E_{CC3/apVTZ} - E_{CCSD/apVTZ}). \tag{1.15}$$

The energy points are fitted by a least-squares method to the force constants. A refit produces the QFF minimum equilibrium geometry and the zero-point force constants. The new force constants are converted to Cartesian coordinates through the INTDER program[87]. Subsequently, second-order rotational[64,88] and vibrational[89] perturbation theory (VPT2) computations are employed through the SPECTRO program to produce spectroscopic constants and anharmonic vibrational frequencies[90]. The resulting rovibrational data is used with great success in revealing previously unobserved vibrational modes and reproducing experimental frequencies[65,91,92]. All electronic structure computations are conducted through the PSI4 program[93] except for DK and DKr which uses MOLPRO2010.1[94].

Chapter 2

Symmetry Breaking and Spectral Considerations of the Surprisingly Floppy c-C_3H Radical and the Related Dipole-Bound Excited State of c-C_3H^-

2.1 Introduction

Carbon is the fourth most abundant element found in the universe and is an integral part of the scientific understanding of life.[95,96] The capacity for carbon to form chains is crucial to the development of life and the primary atomic make-up of interstellar molecules. Despite the high abundance of hydrogen, the majority of molecular species throughout the interstellar medium (ISM) are largely made-up of carbon due to its special bonding properties. This has brought about significant attention from the astrochemical community in order to explore the various ways in which carbon-rich molecular species can form, react, exist, and be detected in the ISM.[97]

One set of molecules of interest are the C_nH chain radicals. This class of molecules plays an important role as reactive intermediates in combustion chemical networks and the chemistry of the ISM.[98] Eight of these radicals have been detected in the ISM including: CH, C_2H, C_3H, C_4H, C_5H, C_6H, C_7H, and C_8H.[98–106] The C_3H radical, which is the primary focus of this paper, is believed to be prevalent throughout the ISM reaching fractional abundances of 10^{-9} compared to hydrogen.[107–109] This radical has been shown to be a product of carbon chain growth via photochemical reactions in interstellar clouds[97,110] and may be part of a cyclopropanylidene (c-C_3H_2) reaction scheme potentially leading to the formation of polycyclic aromatic hydrocarbons (PAHs).[8,9]

C_3H is known to have two isomers in the l-C_3H and c-C_3H forms. The linear propanylidenyl radical form was observed in the laboratory via microwave spectroscopy.[107] and detected in interstellar clouds and circumstellar envelopes in 1985.[111] Soon after, c-C_3H was created in the laboratory and subsequently detected in the dark molecular cloud found in the constellation Taurus, TMC-1, in 1987.[112] Previous work has shown that the relative abundance of the cyclic form is predicted to be roughly three times higher than that of the linear within TMC-1. Furthermore, c-C_3H has been shown to be slightly more abundant than c-C_3H_2[6,7] indicating that this radical may yet be of vital importance in interstellar organic chemistry.

The cyclic isomer has a C_{2v}[113] geometry and a $\tilde{X}\ ^2B_2$ ground electronic state.[114] However, this arrangement may be short lived since the distortion of the carbon ring due to the C$-$C antisymmetric stretch breaks the geometry from C_{2v} to C_s. Previous work has provided rotational constants and geometrical data with some inconsistency.[115] Early experimental observations predict the preferred geometry for c-C_3H to be C_s rather than C_{2v}. The argument is that the cyclic radical has two

equivalent C_s minima that act as a resonance structure with a C_{2v} intermediate.[108] This effect leads to a strong pseudo Jahn-Teller effect in which the orbital mixing of the symmetry-broken states is significant whereas the higher-symmetry geometry forbids such mixing. For c-C_3H, this distortion is due to the symmetry labels for highest occupied molecular orbital (HOMO, b_2) and HOMO-1 (a_1)[116,117] both becoming a' orbitals[114] upon symmetry breaking.

Even so, experiment has been able to observe the ground rotational constants for c-C_3H,[112], but none of the vibrational frequencies have been explicitly established.[118] Computation has only been able to provide some of the vibrational data useful for any possible experimental detection and none at high-level with anharmonic corrections.[114,118] There exists notable discrepancies concerning the computed harmonic vibrational frequencies. The disparity between the data is most likely due to the difference in the computational methods utilized and their ability to treat "atypical" chemistry.

B3LYP has been used with great success for many small molecules, but it is not consistent in the description of the fundamental vibrational frequencies for c-C_3H with higher levels of theory[118] Moreover, the more trustworthy equation of motion ionization potential-coupled cluster singles and doubles method (EOMIP-CCSD) has been useful in producing a more complete discussion of the structural and vibrational data for c-C_3H.[114] The differing results are discussed later in comparison to the present $ab\ initio$ calculations.[114,118] Furthermore, the work presented here uses highly accurate quartic force fields (QFFs) computed using the "gold standard" of computational methods, coupled cluster singles, doubles, and perturbative triples [CCSD(T)].[57,79] QFFs are used to calculate vibrationally-averaged equilibrium geometries, spectroscopic constants, and vibrational

frequencies building upon much previous success with frequencies deteremined to within 1.0 cm^{-1} of experiment in many cases.[29,31,33,35–37,119]

Furthermore, the c-C_3H radical has been proposed to be the precursor for the formation of the closed-shell anion c-C_3H^- [71,118] in the ISM. The suggested creation pathway for the anion is through a dipole-bound excited state intermediate.[34,71,120–122] This dipole-bound excited state (DBXS) mechanism requires the neutral radical to posses a dipole moment of greater than at least 2.0 D.[123,124] The c-C_3H radical is thought to be a good candidate for this mechanism due to its adequate dipole moment of $\sim$ 2.3-2.5 D[114,118] and notable interstellar abundance. The magnitude of the dipole moment is crucial to the DBXS mechanism since the intermediate state is created when the positive end of the dipole field captures a free electron in a highly diffuse quasi-Rydberg state. Subsequently, the ground state closed-shell anion is formed when the DBXS intermediate releases a photon and the trapped electron pairs with the free radical. If c-C_3H^- is to be observed in the ISM, as has been suggested from the computation of its rovibrational properties,[71] further understanding of the neutral radical and its potential DBXS will aid in its chemical classification.

Consequently, the present work will analyze the electronic structure of c-C_3H with an eye toward its rovibrational properties. The behavior of the antisymmetric stretch will be scrutinized, and the fundamental vibrational frequencies, notably the C$-$H stretch, C$-$C symmetric stretch, H$-$C$-$C symmetric bend, and the out-of-plane motion, will be provided for the very first time. These data will inform both laboratory and astronomical observations of the molecule especially with the current growth in infrared telescopic power brought about by the upcoming launch of the James Webb Space Telescope.

2.2 Computational Details

Geometry optimizations for the $\tilde{X}\ ^2B_2$ ground state of the c-C_3H neutral radical are computed under the restricted open-shell Hartree-Fock[50] reference wavefunction with CCSD(T)[56–58,63] using the aug-cc-pV5Z[80,81] basis set.[83] The final reference geometry for the neutral radical is computed by adding the difference in geometrical parameters for the Martin-Taylor (MT) basis set[82] with and without core electron contribution to the aug-cc-pV5Z results.[67] The composite CcCR reference geometry is calculated using the following form with R representing some geometrical component:

$$R = R_{5Z} + (R_{MTc} - R_{MT}). \tag{2.1}$$

The spectroscopic data produced in this work are computed, again, using QFFs which accurately define the potential energy surfaces (PESs) for the anharmonic internuclear potential.[65] QFFs are fourth-order Taylor series expansion approximations to the potential of the internuclear Hamiltonian and are defined as,

$$V = \frac{1}{2}\sum_{ij} F_{ij}\Delta_i\Delta_j + \frac{1}{6}\sum_{ijk} F_{ijk}\Delta_i\Delta_j\Delta_k + \frac{1}{24}\sum_{ijkl} F_{ijkl}\Delta_i\Delta_j\Delta_k\Delta_l \tag{2.2}$$

with displacements of Δ_i and force constants in terms of $F_{ij...}$.

The ground state QFF for the closed-shell anion has been provided from previous work.[71] In order to examine the possible $1\ ^1B_2$ DBXS excited state of the anion, CCSD(T) can no longer serve

as the base method leaving CCSD as the method required. Rovibronic data is computed from the difference between rovibrational levels of the ground and excited states at the same level. Hence, CCSD-based computations must be performed for both the ground and excited state with the same level of theory. The corresponding CcCE geometry for the ground and excited state is computed as,[67,86]

$$R = R_{5Z} + (R_{MTc} - R_{MT}) + (R_{CC3/TZ} - R_{CCSD/TZ}). \tag{2.3}$$

The computations involving the $1\ ^1\mathrm{B}_2$ excited state of tc-$\mathrm{C_3H^-}$ utilize EOM-CCSD instead of simple CCSD. Furthermore, all of the basis sets used for the anionic excited state, whether in the geometry or in the single point energy computations, are also augmented to use additional $6s$, $6p$, and $2d$ diffuse, hydrogen-type functions centered on the H atom to treat the highly diffuse nature of the dipole-bound excitation. These functions are constructed in an even-tempered fashion like those established previously.[125]

The final composite reference geometry for any QFF flavor of a molecule with this connectivity is used to generate energy points defined from the following symmetry-internal coordinates

similar to those previously defined for c-C_3H^-:[71]

$$S_1 = (C_1 - H) \tag{2.4}$$

$$S_2 = \frac{1}{\sqrt{2}}[(C_1 - C_2) + (C_1 - C_3)] \tag{2.5}$$

$$S_3 = \frac{1}{\sqrt{2}}[\angle(H - C_1 - C_2) + \angle(H - C_1 - C_3)] \tag{2.6}$$

$$S_4 = \frac{1}{\sqrt{2}}[(C_1 - C_2) - (C_1 - C_3)] \tag{2.7}$$

$$S_5 = \frac{1}{\sqrt{2}}[\angle(H - C_1 - C_2) - \angle(H - C_1 - C_3)] \tag{2.8}$$

$$S_6 = OPB\angle(H - C_1 - C_2 - C_3). \tag{2.9}$$

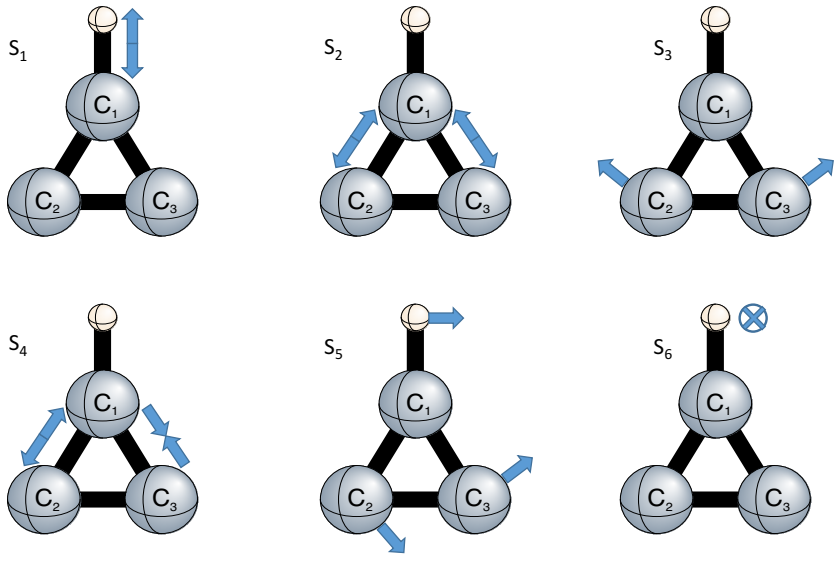

Figure 2.1: Corresponding physical effects of the Symmetry Internal Coordinates on c-C_3H

Moreover, the physical effects of the symmetry-internal coordinates S_1 through S_6 are visually

represented in Figure 2.1.

The notation OPB is defined as the out-of-plane bend. A total of 413 points define the QFF.[65] The QFF is generated by the displacement, from Equation 2.2, of each bond length, angle, and torsion by 0.005 Å or 0.005 radians depending upon the unit in question. At each point for the ground state computations, seven energy computations are performed with CCSD(T). Energies from the aug-cc-pVTZ, aug-cc-pVQZ, aug-cc-pV5Z basis sets are extrapolated to the one-particle complete basis set (CBS) limit by a three-point formula.[84] The newly computed CBS energy is corrected for scalar relativistic effects[85] as well as core correlation again from the MT basis set.[82] This results in the so-called CcCR QFF discussed elsewhere.[70,126] The CcCR QFF composite energy scheme is as follows;[67]

$$E_{CcCR} = E_{CBS} + (E_{MTc} - E_{MT}) + (E_{apVTZ-DKr} - E_{apVTZ-DK}). \tag{2.10}$$

When the level of theory for the QFF is reduced from CCSD(T) to CCSD, the relativistic corrections are eliminated and replaced with a correlated triples correction, CC3,[127–129] by following the CcCE QFF scheme;[67]

$$E_{CcCE} = E_{CBS} + (E_{MTc} - E_{MT}) + (E_{CC3/apVTZ} - E_{CCSD/apVTZ}). \tag{2.11}$$

The CcCE QFF scheme is used for both the CCSD ground and excited states of the anion as well as the ground state of the neutral radical. The fitting of the CcCE QFF computed with the

three-point CBS limit is unstable likely due to overpowering the basis set for the CCSD level of theory. Removing the aug-cc-pV5Z energy set and using a two-point CBS extrapolation with the aug-cc-pVTZ and aug-cc-pVQZ energies gives more well-behaved data. The notation CcCR(TQ5) or CcCE(TQ), shown later in the data tables, is used to represent the type of CBS extrapolation used, 3-point or 2-point, receptively.

The QFF is then fit through a least squares approach to produce the new minimum geometry. Refitting the QFF zeroes the gradients and produces the most accurate second-, third-, and fourth-order force constants. The INTDER program[87] transforms the QFF into Cartesian coordinates. The spectroscopic constants and anharmonic vibrational frequencies are computed using the SPECTRO program[90]. The program uses vibrational[89] and rotational[64,88] perturbation theory at second-order (VPT2). c-C_3H requires the input of a ν_3/ν_5 Darling-Dension resonance; $2\nu_2 = \nu_1$, $2\nu_6 = \nu_2$, and $2\nu_4 = \nu_3$ Fermi type-1 resonances; and a ν_4/ν_3 Coriolis resonance.

A special potential energy surface (PES) is computed to paint a more clear picture of the problems produced by the pseudo Jahn-Teller effect. The PES is constructed to calculate a one-dimensional PES cut for the symmetry internal coordinate S_4 which corresponds to the antisymmetric C$-$C stretch. 103 points of the PES are computed with the EOM-CCSD/aug-cc-pVTZ level of theory over a 0.0 to 0.6 Å range of displacements for S_4. Most displacements are or 0.005 Å, but some areas require displacements as small 0.001 Å in order to properly characterize this PES cut. The calculations are used to provide energies for the ground state and three of the five lowest lying excited states along with the molecular orbitals and the T_1 and D_1 diagnostics for detecting any multireference character.[130]

2.3 Results and Discussion

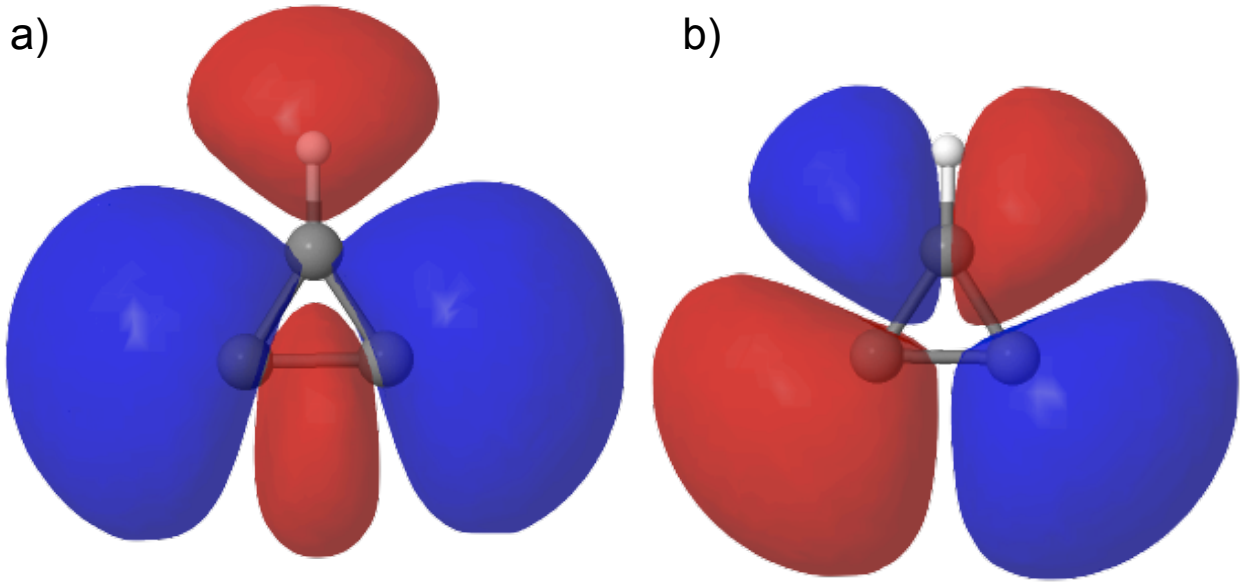

Figure 2.2: Visualization of the Molecular Orbitals for c-C_3H Radical: a) a_1 HOMO-1 and b) singly-occupied b_2 HOMO.

The $\tilde{X}\ ^2B_2$ ground electronic state of c-C_3H radical has a (core)$3a_1{}^2\ 4a_1{}^2\ 2b_2{}^2\ 5a_1{}^2\ 1b_1{}^2\ 6a_1{}^2\ 3b_2$ orbital occupation with the HOMO only being half-filled. A visual representation of the actual b_2 HOMO and a_1 HOMO-1 of the $\tilde{X}\ ^2B_2$ ground state is shown in Figure 2.2b and 2.2a, respectively. The difference in energy between these two orbitals is -5.67 eV. The HOMO, seen in Figure 2b, is the singly-occupied b_2 orbital. The half filled HOMO of the ground state is a source of complication when breaking the symmetry from C_{2v} to C_s. When the symmetry breaks, the radical in the HOMO moves from the b_2 labeled orbital into an a' orbital that occupies similar space and has the same symmetry label.

2.3.1 Geometry and Spectroscopic Data

The CcCR(TQ5), or just CcCR, QFF computed zero-point and equilibrium geometry as well as rotational constants for the c-C_3H radical are listed in Table 2.1. The agreement between the computed vibrationally-averaged (R_α) zero-point rotational constants and those observed through microwave spectroscopic experiment,[108] also reported in Table 2.1, is supportive of promising results. There is a difference less than 1% in the A_0, and the B_0 and C_0 differ from experiment by approximately 204 MHz and 97 MHz, respectively. The slight discrepancy between the presented rotational constants and experiment can be attributed to the similar differences in the geometrical data. These deviations are not very large. For example, the computed zero-point C−H bond distance differs from the experimental value by 0.001 Å and the C−C bond distance only differs by 0.004 Å. Thus, our data are in good agreement with known experimentally observed values.

The structural data produced in this study for c-C_3H are also compared to previous theoretical data[114,118] in Table 2.1. The equilibrium C−H bond distance produced in this study, 1.077 Å, is 0.002 Å lower than the B3LYP/aug-cc-pVTZ value reported at 1.079 Å. On the other hand, the C−C bond distance is 0.004 Å greater.[118] The B3LYP/aug-cc-pVTZ equilibrium bond angle differs from the CcCR by 0.01°. The EOMIP-CCSD/aug-cc-pVTZ zero-point geometry computed in an earlier theoretical study[114] is in close agreement with the CcCR QFF zero-point geometry from the current study. The zero-point C−H and C−C bond distances differ by 0.003 Å and 0.001 Å, respectively. This overall agreement in the geometry and rotational constants with previous

Table 2.1: The Geometry, Spectroscopic Constants, and Vibrational Frequencies (Intensities in Parentheses) for the c-C_3H Radical and Anion

	c-C_3H					c-C_3H^-	
	CcCR(TQ5)	CcCE(TQ)	Previous Theory		Exp[c]	CcCR(TQ5)[d]	CcCE(TQ)
r_0(C−H) Å	1.077 087	1.079 220	1.0741[a]		1.0760	1.088 094	1.087 063
r_0(C−C) Å	1.377 953	1.376 938	1.3718[a]		1.3739	1.380 838	1.384 245
$\angle_0$(H−C−C) rad	149.997	150.022				147.291	146.841
r_e(C−H) Å	1.077 485	1.077 486	1.079[b]			1.085 088	1.084012
r_e(C−C) Å	1.373 416	1.372 311	1.369[b]			1.373 928	1.377176
$\angle_e$(H−C−C) rad	150.068	150.072	150.2[b]			147.293	146.843
A_e MHz	44 839.68	44 921.15				38 207.91	37 116.06
B_e MHz	34 227.96	34 273.69				35 921.83	36 100.79
C_e MHz	19 410.86	19 440.83				18 514.81	18 300.69
A_0 MHz	44 582.08	44 626.51			44 536.82	38 023.29	36 926.36
B_0 MHz	34 211.66	34 153.23			34 016.34	35 723.74	35 894.77
C_0 MHz	19 285.76	19 316.62			19 188.85	18 351.90	18 136.16
A_1 MHz	44 543.33	44 587.23				37 886.04	36 794.51
B_1 MHz	34 043.37	33 982.74				35 619.47	35 788.37
C_1 MHz	19 225.02	19 254.72				18 292.96	18 077.73
A_2 MHz	44 354.58	44 395.56				37 921.12	36 825.86
B_2 MHz	34 082.55	34 022.25				35 535.80	35 703.42
C_2 MHz	19 203.46	19 231.09				18 288.98	18 058.34
A_3 MHz	44 926.15	44 626.51				38 281.39	37 166.09
B_3 MHz	34 280.57	34 153.23				35 465.07	35 629.59
C_3 MHz	24 355.60	19 316.62				18 339.12	18 134.82
A_4 MHz	44 250.17	44 289.28				37 528.18	36 447.27
B_4 MHz	34 313.59	34 255.16				36 081.43	36 264.97
C_4 MHz	14 146.99	19 222.94				18 153.62	17 942.04
A_5 MHz	44 573.04	48 919.05				37 835.91	36 737.33
B_5 MHz	34 349.41	34 156.07				35 618.23	35 777.29
C_5 MHz	19 223.46	19 285.70				18 372.85	18 152.53
A_6 MHz	44 329.84	40 352.32				38 317.87	37 207.76
B_6 MHz	34 168.38	34 108.73				35 626.22	35 792.93
C_6 MHz	19 309.41	19 340.37				18 337.97	18 122.32
D_J MHz	0.022 161	0.055 937				0.053	0.054 591
D_{JK} MHz	0.367 680	-0.155 802				0.070	0.059 603
D_K MHz	-0.178 034	0.314 383				0.123	0.112 641
d_1 MHz	-0.019 897	-0.020 072				-0.029	-0.030 058
d_2 MHz	-0.015 176	0.001 466				-0.009	-0.009 250
H_J Hz	-0.522 264					0.179	0.111 003
H_{JK} Hz	5.926 119					-6.906	-0.063 767
H_{KJ} Hz	-3.555 337					24.229	0.002 324
H_K Hz	-1.671 141					-17.601	-0.001 712
h_1 Hz	-0.058 135					0.021	1.484 238
h_2 Hz	0.337 861					0.153	0.199 989
h_3 Hz	0.134 148					0.221	0.241 217
Harmonic Zero-Point cm^{-1}	4386.1					4258.7	4255.5
ω_1 (a_1) cm^{-1} C−H	3256.8 (0)	3259.8	3330[a]	3222[b]		3100.2	3101.1
ω_2 (a_1) cm^{-1} C−C sym. stretch	1588.6 (4)	1583.1	1639[a]	1616[b]		1507.0	1496.7
ω_3 (a_1) cm^{-1} H−C−C sym. bend	1219.5 (16)	1215.9	1244[a]	1236[b]		905.1	902.7
ω_4 (b_2) cm^{-1} C−C antisym. stretch	619.5 (18)	927.7	281[a]	578[b]		838.8	841.1
ω_5 (b_2) cm^{-1} H wag	1224.8		958[a]	921[b]		1297.2	1300.3
ω_6 (b_1) cm^{-1} ∠OPB	863.1 (6)	864.8	898[a]	879[b]		869.1	869.2
Anharmonic Zero-Point cm^{-1}	4290.2					4088.5	3905.1
ν_1 (a_1) cm^{-1}	3117.7	3116.6				2950.4	2942.2
ν_2 (a_1) cm^{-1}	1564.3	1556.0				1475.9	1461.4
ν_3 (a_1) cm^{-1}	1198.5	1200.5				876.6	852.4
ν_4 (b_2) cm^{-1}	662.6					763.8	462.8
ν_5 (b_2) cm^{-1}	1210.6					1267.1	1265.5
ν_6 (b_1) cm^{-1}	826.7	788.6				843.1	825.8

[a] EOMIP-CCSD/aug-cc-pVTZ results from Ref. 114.
[b] B3LYP/aug-cc-pVTZ results from Ref. 118.
[c] Microwave Spectroscopy results from Ref. 108.
[d] CcCR results from Ref. 34.

theory and experiment leads to confidence in the other CcCR QFF computed data for which there are fewer benchmarks.

Although the CcCR QFF data is sufficient for the characterization of c-C_3H, a CcCE(TQ), which will be referred to as CcCE from hereon, QFF is computed for comparison and benchmarking of the method. The CcCE(TQ) QFF of c-C_3H is in excellent agreement with the CcCR QFF. Similarly, the CcCR and CcCE data for c-C_3H^- are also in excellent agreement and will be discussed later. This agreement indicates the lower level of theory may be adequate for the characterization of some states or species that may forbid the use of CCSD(T), like the use of coupled cluster excited state computations where CCSD(T) cannot be utilized because no explicit wavefunction can be defined.

Table 2.2: The CcCR QFF c-C_3H Simple-Internal Force Constants (in mdyn/Å^n·rad^m).

F_{11}	5.707 241	F_{311}	0.3265	F_{2211}	-0.51	F_{5521}	-0.00
F_{21}	0.013 439	F_{321}	-0.1871	F_{2221}	0.89	F_{5522}	1.06
F_{22}	8.989 486	F_{322}	22.0773	F_{2222}	129.34	F_{5531}	0.06
F_{31}	0.156 339	F_{331}	-0.1540	F_{3111}	-0.38	F_{5532}	-0.89
F_{32}	-6.941 876	F_{332}	-66.0232	F_{3211}	-0.14	F_{5533}	8.23
F_{33}	18.743 572	F_{333}	216.6795	F_{3221}	0.49	F_{5555}	0.58
F_{44}	4.934 473	F_{551}	-0.0471	F_{3222}	-57.05	F_{6611}	0.65
F_{54}	0.845 536	F_{552}	-0.4054	F_{3311}	-0.28	F_{6621}	0.92
F_{55}	0.232 560	F_{553}	-0.2040	F_{3321}	0.69	F_{6622}	55.76
F_{66}	0.379 258	F_{661}	0.2714	F_{3322}	146.94	F_{6631}	0.15
F_{111}	-33.1729	F_{662}	-17.5276	F_{3331}	-0.90	F_{6632}	-194.41
F_{211}	0.2341	F_{663}	46.1096	F_{3332}	-487.87	F_{6633}	703.05
F_{221}	-0.4447	F_{1111}	169.49	F_{3333}	2148.80	F_{6655}	2.18
F_{222}	-37.7787	F_{2111}	-1.11	F_{5511}	0.16	F_{6666}	355.25

The CcCR QFF and CcCE QFF simple-internal force constants for c-C_3H are listed in Table 2.2 and Table 2.3, respectively. Note for the CcCE force constants in Table 2.3, any force constant that has a contribution from symmetry-internal coordinate S_4 is not reported due to a problems in

Table 2.3: The c-C_3H Simple-Internal Force Constants using the CcCE QFF(in mdyn/Å^n·rad^m).

F_{11}	5.765 341	F_{331}	-0.1871	F_{3211}	-0.24	F_{5555}	1.59
F_{21}	0.021 503	F_{332}	-67.5007	F_{3221}	0.42	F_{6611}	0.52
F_{22}	9.155 391	F_{333}	-219.6909	F_{3222}	-56.28	F_{6621}	-0.20
F_{31}	0.150 147	F_{551}	-0.0506	F_{3311}	-0.34	F_{6622}	55.25
F_{32}	-7.041 538	F_{552}	-0.3884	F_{3321}	0.80	F_{6631}	0.11
F_{33}	18.939 417	F_{553}	-0.3103	F_{3322}	145.05	F_{6632}	-192.11
F_{55}	0.234 845	F_{661}	0.2426	F_{3331}	-0.74	F_{6633}	685.79
F_{66}	0.384 905	F_{662}	-17.7973	F_{3332}	-484.50	F_{6655}	1.59
F_{111}	-33.6076	F_{663}	46.6497	F_{3333}	2120.73	F_{6666}	338.77
F_{211}	0.1640	F_{1111}	166.77	F_{5511}	1.12		
F_{221}	-0.4906	F_{2111}	-1.01	F_{5521}	0.05		
F_{222}	-38.7387	F_{2211}	-0.43	F_{5522}	0.19		
F_{311}	0.3502	F_{2221}	1.20	F_{5531}	0.01		
F_{321}	-0.1662	F_{2222}	127.73	F_{5532}	7.01		
F_{322}	22.6596	F_{3111}	-0.24	F_{5533}	-0.26		

the electronic structure of this mode, as explained later in the manuscript. The relative differences between the CcCR and CcCE diagonal harmonic force constants are minimal, with the largest harmonic discrepancies in F_{22} and F_{33} of 0.017 mdyne/Å^2 and 0.20 mdyne/Å^2 respectively. The remaining force constants F_{11}, F_{55}, and F_{66} are in excellent agreement with with discrepancies of 0.06 mdyne/Å^2, 0.00 mdyne/Å^2, and 0.01 mdyne/Å^2.

2.3.2 Vibrational Frequencies

The harmonic and anharmonic vibrational frequencies for the $\tilde{X}\ ^2B_2$ ground state of c-C_3H are also listed in Table 12.1, again with comparison to data from previous theory.[114,118] The ω_1 harmonic C$-$H stretching vibrational mode computed in this study, 3256.8 cm^{-1}, is 73 cm^{-1} lower than the EOMIP-CCSD value of 3300 cm^{-1} but still in quite reasonable agreement. Likewise,

the CcCR ω_2 is 50.4 cm^{-1} lower than the EOMIP-CCSD value, and there is similar agreement with the ω_6 OPB fundamental mode. The CcCR ω_3 symmetric bend at 1219.5 cm^{-1} is actually the most consistent with the EOMIP-CCSD computations where the latter value is 1244 cm^{-1}. However, significant disagreement does arise in the C$-$C antisymmetric stretch mode, ω_4. The EOMIP-CCSD study[114] reports ω_4 as 281 cm^{-1}, while the CcCR value is 619.5 cm^{-1}. The varied discrepancy is indicative of an issue in defining the molecular wavefunction for c-C_3H for reasons to be discussed later. The CcCR in-plane hydrogen wag (H$-$C$-$C antisymmetric bend) motion, ω_5 is computed to be 1224 cm^{-1} where the EOMIP ω_5 is reported to be 898 cm^{-1}. As a result, the a_1 and b_1 modes appear to be well-described in the present work, while the b_2 modes are more problematic.

Furthermore, the reported CcCR harmonic vibrational frequencies for ω_1, ω_2, ω_3, and ω_6 are in good agreement with the values reported from the earlier B3LYP/aug-cc-pVTZ study,[118] with differences of 34.8 cm^{-1}, 27.4 cm^{-1}, and 15.9 cm^{-1} respectively. The previously computed B3LYP values for ω_4 and ω_5 remain the most worrisome with large discrepancies compared to the values computed here. However, ω_4 varies between the B3LYP and EOMIP-CCSD values, as well. The B3LYP ω_4 is reported to be 578 cm^{-1} where the CcCR value is lower at 619.5 cm^{-1}. This is a relatively small difference, but, again, neither are in a similar frequency range as EOMIP-CCSD. Furthermore, the CcCR value of ω_5 is 1224.8 cm^{-1} which is higher than the B3LYP reported value reported to be 921 cm^{-1}. Again, the a_1 and b_1 modes behave well, but the b_2 modes offer questions in both the CcCR and B3LYP computations.

Although there are some large discrepancies between the CcCR harmonics reported in this

study and harmonics provided by previous theories, the CcCR harmonic vibrational frequencies computed here are actually in excellent agreement with the CcCE harmonic vibrational frequencies, especially, again for the a_1 and b_1 modes. The ω_5 H$-$C$-$C antisymmetric bending vibrational mode is not reported for the CcCE method due to significant numerical noise in the computation. The lower level of theory struggles to define the wavefunction upon b_2 distortion which is a clear indicator of multireference character where triples-including methods, at the very least if not static correlation methods, must be included.[131] Again, this will be discussed later in more detail. However, the CcCE harmonic vibrational frequencies ω_1, ω_2, ω_3, and ω_6 are reported with minimal discrepancies relative to the corresponding CcCR values. As seen in Table 2.1, the CcCR and CcCE ω_1 are within 3 cm^{-1} of each other supporting the claim for the effectiveness of the lower level of theory in describing behavior where single-reference methods are fitting and perturbative triples are unavailable. The largest of the CcCR-CcCE discrepancies is between the reported values for ω_2 which is a mere 5.5 cm^{-1}. The differences between CcCR and CcCE modes ω_3 and ω_6 are 3.6 cm^{-1} and 1.7 cm^{-1} respectively.

Perhaps the most important values reported in this work are the CcCR anharmonic vibrational frequencies for the a_1 and b_1 modes. High-level computed values have not been reported in any theoretical study of c-C_3H, and its fundamental vibrational frequencies have not been observed experimentally. While an "experimental" ν_4 has been claimed,[108] this value is derived from the rotational distortions and not from direct observation. Part of the reason that these modes have not been directly observed in the infrared may be due to low intensities of these fundamental frequencies. For instance, the C$-$H stretch has no intensity from trusted[132] MP2/6-31+G* double-harmonic

intensities computed with Gaussian09.[133–135] The most intense trusted band is the H−C−C symmetric bend with an intensity of only 16 km/mol. The others that could be produced are listed in Table 2.1.

The CcCR anharmonic vibrational frequencies for the a_1 and b_1 (ν_1, ν_2, ν_3, and ν_6) fundamentals are the most valuable data points in this work since none have been provided experimentally or theoretically. Furthermore, the spectroscopic constants compare well with experiment, the harmonics for these symmetries are in good agreement with previous theory, and this methodology has performed well in the past even for carbon-containing rings like c-SiC_2.[119] The values of ν_1, ν_2, ν_3, and ν_6 are 3117.7 cm^{-1}, 1564.3 cm^{-1}, 1198.5 cm^{-1}, and 826.7 cm^{-1}, respectively, with the anharmonicities falling within the expected range for each type of mode. Furthermore, the CcCE anharmonic vibrational frequencies are in excellent agreement with the a_1 symmetry-mode CcCR values, differing by 1.1 cm^{-1}, 7.7 cm^{-1}, and 2.0 cm^{-1}, respectively. The difference between the b_1 ν_6 CcCR and CcCE anharmonic vibrational frequency is a somewhat disappointing 38.1 cm^{-1}, but this is not extreme in light of the change in theory. The b_2 CcCE ν_4 and ν_5 anharmonic frequencies are not reported here due to instabilities in this portion of the wavefunction. The CcCR ν_5 appears well-behaved, but if the harmonic computations are off, then the anharmonic will be, as well. Hence, the CcCR ν_4 and ν_5 modes are not trusted.

2.3.3 Pseudo Jahn-Teller Effect

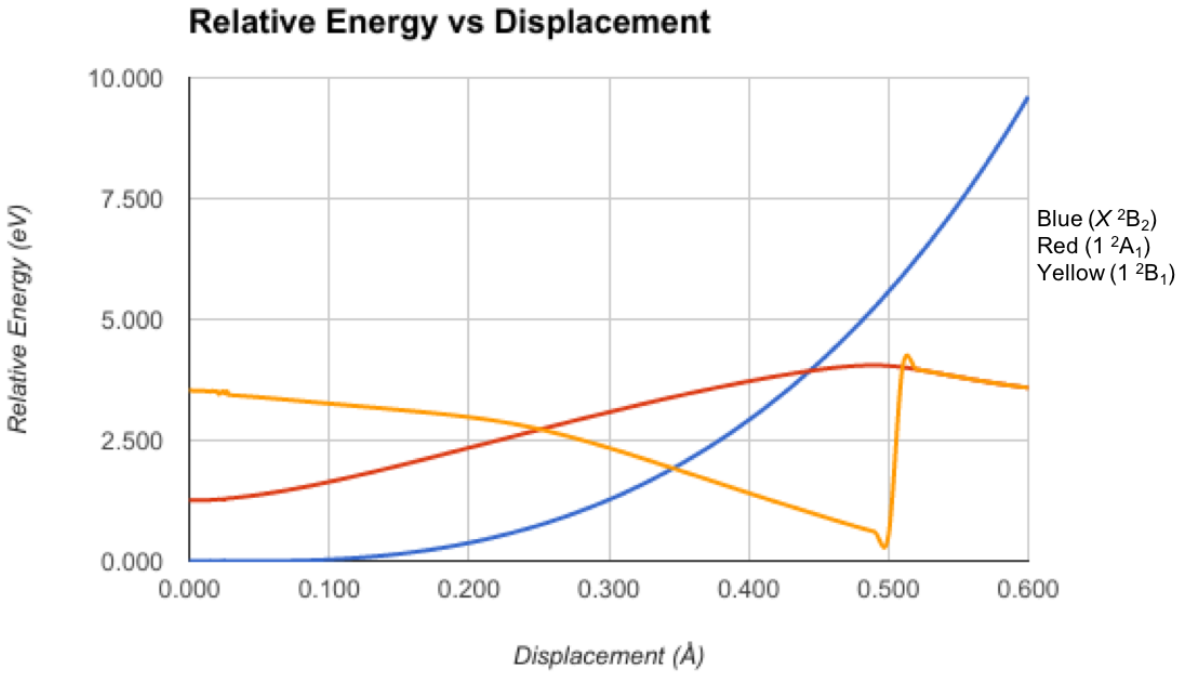

Figure 2.3: Relative energy plot for the $\tilde{X}\ ^2\mathrm{B}_2$ (ground), $1\ ^2\mathrm{A}_1$ (first excited), and $1\ ^2\mathrm{B}_1$ (third excited) with respect to the displacement of symmetry-internal coordinate S_4.

2.3.4 The b_2 Antisymmetric C−C Stretching Surface

The varied discrepancies between the CcCR QFF data produced within this study and the data reported from previous theory is likely caused by the presence of a known[114] pseudo Jahn-Teller effect in c-C_3H. In an attempt to further qualify the presence of this effect, a PES scan is performed to take a more specific look at the localized energy surface for the $S_4(b_2)$ symmetry-internal coordinate, the C−C antisymmetric stretch, in c-C_3H. This mode is chosen because it has the most varied results between CcCR, CcCE, EOMIP-CCSD, and B3LYP. The ground $\tilde{X}\ ^2B_2$, first excited $1\ ^2A_1$, and third excited $1\ ^2B_1$ states are scrutinized and displayed in Figure2.3.

Likely, the most important result from Figure 2.3 is the incredibly flat surface on the bottom blue line for the $\tilde{X}\ ^2B_2$ ground state between 0.000 Å and 0.070 Å. The CCSD/aug-cc-pVTZ energy relative to the C_{2v} structure fluctuates between a mere 0.006 eV and -0.003 eV in this range. In truth, this scan supports the claim of c-C_3H as a resonance of two C_s structures[108] with a minimum of -0.003 eV appearing at 0.044 Å of S_4. However, such a small energy range of less than 0.010 eV is hardly enough to classify this structure as a true double-well potential. The question then is asked of the computations, what is flat? If accuracies can only be claimed at the 0.1 eV level, then the potential could be thought of simply as flat. Hence, the distortion of the ring will largely be barrierless within the first 0.1 Å making this molecule quite floppy. However, a full vibrational frequency analysis will require the potential surface to scan beyond this point, and our QFF approach utilized here does not.

Before moving beyond 0.1 Å, the space before then still has some interesting results. The T_1

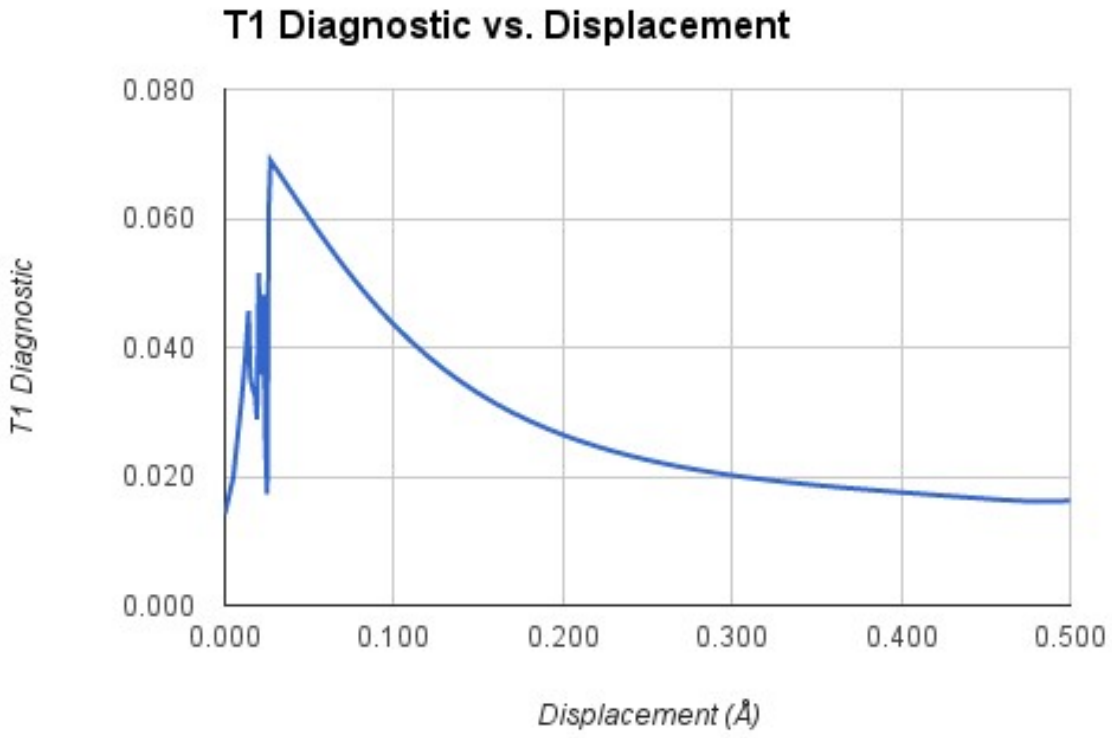

Figure 2.4: Plot of the T_1 diagnostic versus displacement of S_4.

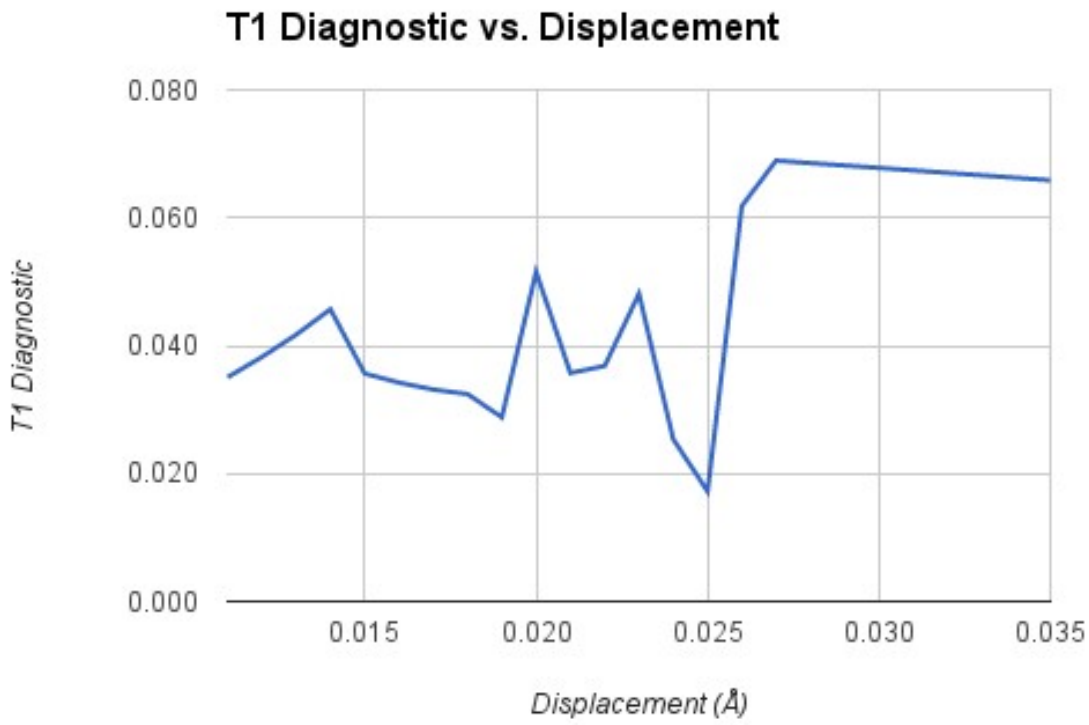

Figure 2.5: Zoom in for the plot of the T_1 diagnostic versus displacement of S_4.

diagnostic is also plotted with respect to S_4 in Figure2.4 and zoomed in on the 0.010 Å to 0.035 Å range in Figure2.5. Immediately after the symmetry is broken to a C_s structure, the T_1 diagnostic grows from a treatable[130] 0.014 to 0.020 in the first 0.005 Å S_4 displacement. In this coordinate, the carbon atoms involved are moving by 0.003 Å each with one toward and one away from the central carbon atom. At 0.010 Å of S_4, T_1 is now into the realm of multireference at 0.032 with the actual atomic positions changing by less than 0.01 Å. Figure 2.5 shows how the T_1 diagnostic fluctuates until 0.027 Å displacement of S_4. Beyond here, the T_1 diagnostic is well-behaved and converges back down to 0.017, below the 0.02 threshold. The D_1 diagnostics behave in near-quantitatively the same manner.

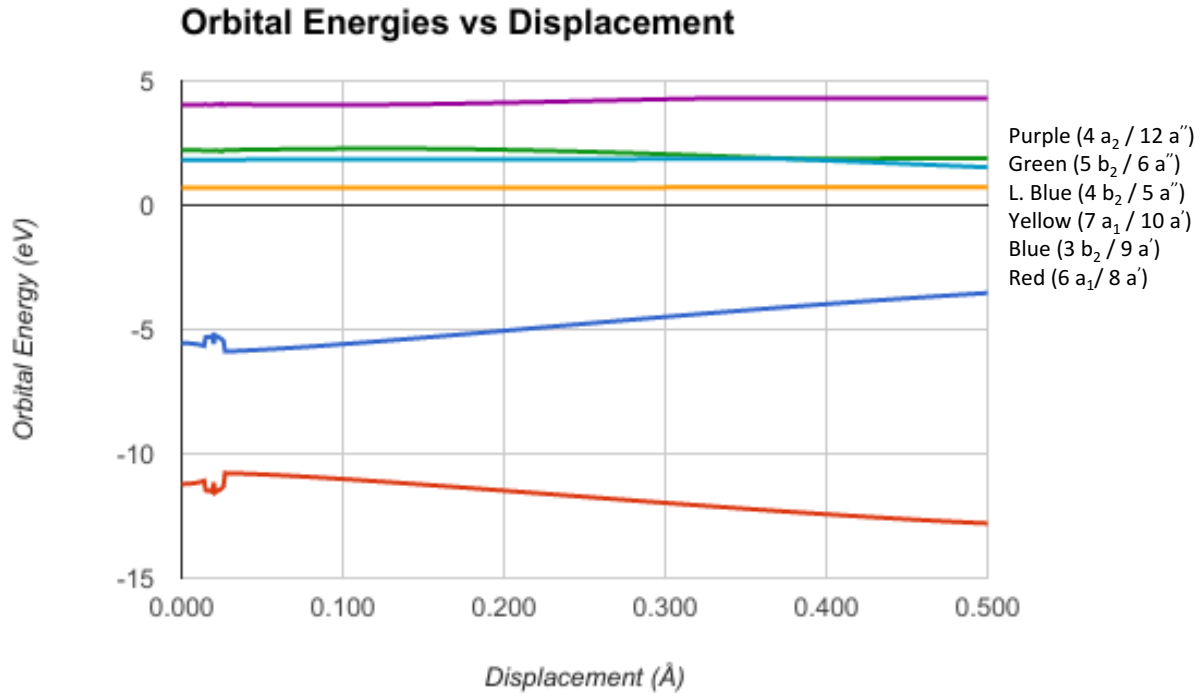

Figure 2.6: Walsh diagram for the $6a_1/8a'$ (HOMO-1), $3b_2/9a'$ (HOMO), $7a_1/10a'$ (LUMO), $4b_2/5a''$, $5b_2/6a''$, and $4a_2/12a''$ orbital energies in relation to displacements of the symmetry-internal coordinate S_4.

The ground and even excited state energies display a fluctuation in this range as well in Figure 2.3, but so do the molecular orbitals, specifically the HOMO and HOMO-1 (red and blue curves) in the Walsh diagram given in Figure 2.6. It is not surprising that the T_1 and D_1 diagnostics fluctuate in chorus with the CCSD energy since both are computed with the same coupled cluster wavefunction, but the fact that the MOs do indicates that the reference is indeed in question in this case. However, in every case described, whether the T_1 values, the energies, or the MOs, the plots stabilize at 0.027 Å in S_4. It is also at this point that the relative energy given in Figure 2.3 actually drops below that of the C_{2v} ground state. Once, the geometry is distorted beyond this narrow region from 0.000 Å to 0.027 Å, the electronic wavefunction is on its way to behaving like a single-reference system once again. It is not until 0.350 Å in S_4 that an excited state is accessed on the PES. At this point, the $1\ ^2B_1$/$2\ ^2A'$ state crosses with the ground state. This state is actually a Rydberg state involving the $3b_2/9a' \rightarrow 7a_1/10a'$ (HOMO $\rightarrow$ LUMO) transition where the $7a_1/10a'$ orbital is Rydberg in nature. Such behavior is logical since two of the carbon atoms in the ring are getting closer together, and the diffuse state allows for the electrons to escape the valence cloud as the nuclear potential increases.

From these plots it is clear that the symmetry breaking has immediate and significant effect on the multireference character and electronic structure of c-C_3H. This is most pronounced in the 0.005 Å to 0.027 Å range with trailing effects still felt until 0.200 Å when T_1 once more falls back under 0.025. At 0.027 Å the potential leading to the shallow but true minimum is finally sampled. From Figure 2.3, it is clear that there is no true state crossing and no orbital occupation shifts from Figure2.6.

The symmetry breaks leading to an indefinite orbital definition since the HOMO and HOMO-1 lie in the same physical space and have the same a' symmetry. Once the ring is sufficiently distorted, the single reference is again sufficient to describe this system. Similar issues have been faced in the $OCHCO^+$ and $NNHNN^+$ proton-bound complexes where the double well and flat potentials forced the QFFs into poor descriptions of modes along such coordinates involving the proton "shuttle" motion. However, other modes were actually quite well described with the CcCR QFF since the higher symmetry "saddle point" was well below the zero-point energy making any physically meaningful predictions of the symmetry-broken structure meaningless.[132,136] Consequently, the ν_1, ν_2, ν_3, and ν_6 CcCR fundamental vibrational frequencies are likely properly described in this system. Any further analysis would require more than a simple QFF for the PES description in any of the b_2 modes. The surface immediately after symmetry breaking would have to be sampled in detail and that after 0.350 Å in S_4 where the Rydberg or ionization is more favored would also have to be effectively treated.

2.3.5 Anion

One of the intended outcomes of this work is to provide evidence about the possible interstellar formation of c-C_3H^- from c-C_3H through a DBXS intermediate. As shown in Figure 2.8, the orbital occupation of the ground state of c-C_3H^- is closed-shell such that the multireference problems described above are not at issue. However, the excitation of the electron out of the HOMO into an s-type virtual orbital (the middle panel of Figure 2.8) produces the $1\ ^1B_2$ DBXS and an

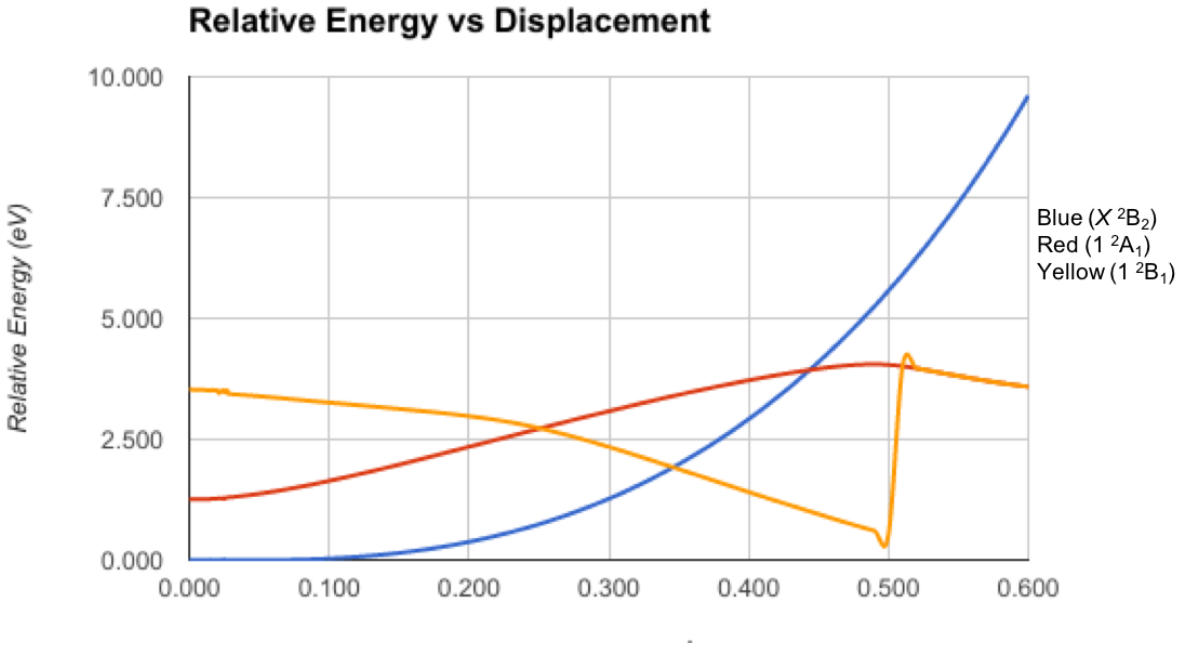

Figure 2.7: Relative energy plot for the $\tilde{X}\ ^2\mathrm{B}_2$ (ground), $2\ ^2\mathrm{A}_1$ (first excited), and $A\ ^2\mathrm{B}_1$ (third Excited) with respect to the displacement of symmetry-internal coordinate S_4.

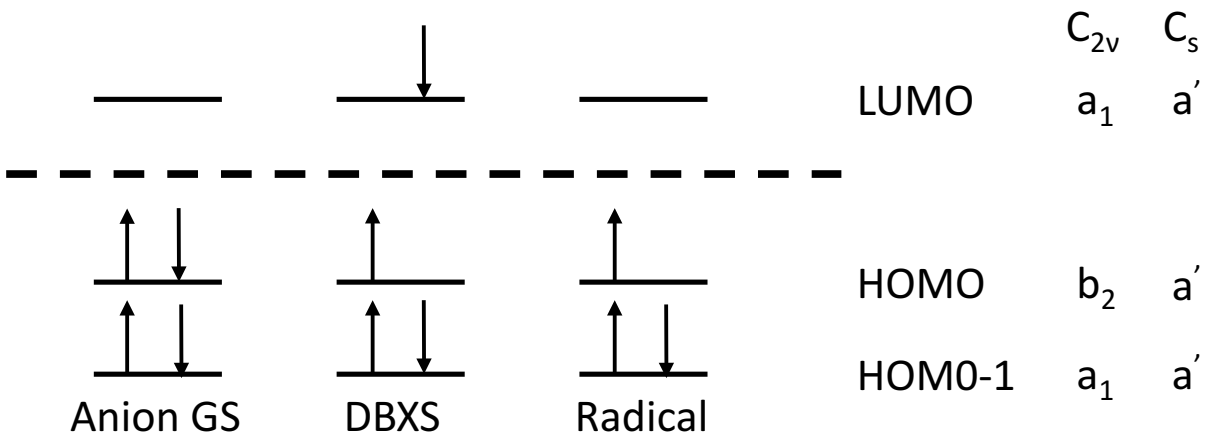

Figure 2.8: Molecular Orbitals for c-$\mathrm{C}_3\mathrm{H}$ Radical, Anion, and Excited State Intermediate

electronic structure much like that of the neutral radical (the right panel of Figure 2.8) since the a_1 LUMO will be quite distant from the molecular core.

Table 2.4: The CcCE c-C_3H^- Simple-Internal Constants (in mdyn/Å^n·rad^m).

F_{11}	5.257 729	F_{441}	-0.0469	F_{3222}	-35.31	F_{5444}	3.53
F_{21}	0.131 062	F_{442}	-27.7160	F_{3311}	0.03	F_{5511}	-0.27
F_{22}	8.326 124	F_{443}	-0.4360	F_{3321}	1.06	F_{5521}	-0.12
F_{31}	0.313 092	F_{541}	-0.3971	F_{3322}	91.73	F_{5522}	0.23
F_{32}	-4.192 169	F_{542}	0.0158	F_{3331}	-0.64	F_{5531}	0.04
F_{33}	9.461 417	F_{543}	-0.8511	F_{3332}	-270.27	F_{5532}	0.42
F_{44}	6.819 573	F_{551}	0.0192	F_{3333}	950.75	F_{5533}	-2.35
F_{54}	-0.030 324	F_{552}	-0.3739	F_{4411}	-1.60	F_{5544}	0.00
F_{55}	0.247 061	F_{553}	-0.7813	F_{4421}	1.15	F_{5554}	0.52
F_{66}	0.364 723	F_{661}	0.5802	F_{4422}	93.76	F_{5555}	-0.22
F_{111}	-32.4027	F_{662}	-9.6656	F_{4431}	-1.93	F_{6611}	1.16
F_{211}	0.3672	F_{663}	20.6155	F_{4432}	22.81	F_{6621}	-0.86
F_{221}	-0.6795	F_{1111}	163.46	F_{4433}	-55.71	F_{6622}	27.94
F_{222}	-34.2325	F_{2111}	-1.30	F_{4444}	84.34	F_{6631}	1.51
F_{311}	0.7032	F_{2211}	-0.68	F_{5411}	-0.61	F_{6632}	-90.16
F_{321}	-0.4851	F_{2221}	1.12	F_{5421}	0.35	F_{6633}	257.37
F_{322}	14.1784	F_{2222}	113.77	F_{5422}	0.14	F_{6644}	0.29
F_{331}	0.2023	F_{3111}	0.08	F_{5431}	-0.39	F_{6654}	-1.86
F_{332}	-40.1180	F_{3211}	-0.55	F_{5432}	1.18	F_{6655}	-1.03
F_{333}	107.8126	F_{3221}	0.93	F_{5433}	-2.91	F_{6666}	110.39

The ground electronic state rovibrational computations of c-C_3H^- have been reported elsewhere,[34] but the CcCE QFF produced geometry, rotational constants, and vibrational frequencies for c-C_3H^- are listed in Table 2.1. The CcCE QFF simple-internal force constants for c-C_3H^- are reported in Table 2.4. The varied, but minimal differences between the CcCR and CcCE data suggest that the CCSD-based approach tested in this study is adequate for characterization of the anion giving strength to any conclusions drawn from CcCE QFFs like those to come for excited states. The one notable exception is the ν_4 C−C antisymmetric stretch. Even though ω_4 is similar, the larger T_1 diagnostics even for the closed-shell anion are problematic for this mode utilized

with only CCSD where the additional dynamic correlation of at least perturbative triples appears to correct some of the issues encountered in the symmetry breaking of the b_2 coordinates.

The EOM-CcCE geometry zero-point and equilibrium geometries, rotational constants, spectroscopic constants, and vibrational frequencies for the $1\ ^1B_2$ DBXS of c-C_3H^- are listed in Table 2.5. The common wisdom is that any DBXS could behave nearly exactly like the corresponding neutral. Hence, this state's values should look almost identical to those of the ground state of the radical. This expectation is supported by the minimal difference between the corresponding bond distances and bond angles of 0.004 Å and 0.3 degrees, respectively. Similarly, the differences in the corresponding rotational constants are within 2%. Only the ω_1, ω_2, ν_1, and ν_2 frequencies can be reported with any level of confidence due to the presence of the same symmetry-breaking issues here as in the ground state of the c-C_3H radical. The force constants utilized to create these data are given in Table 2.6. Only those S_x coordinates that produce viable results are reported, and they are in semi-quantitative agreement as those reported in Table 2.3 for the CcCE QFF of the neutral radical.

The good correspondence in the produced data as well as the presence of the same, frustrating behavior in those observables with b_2 symmetry in both the neutral radical and the DBXS of the anion can actually be taken as a somewhat positive conclusion. They indicate that these two states are, in fact, structurally and electronically similar to one another as has been assumed for such corresponding neutrals and dipole-bound anions. It was hoped that the linear combination of states produced in the EOM wavefunction for the DBXS could serve as a kind of "poor man's" coupled cluster multireference treatment in neutral radicals. However, the additional nuances of

Table 2.5: The Geometry, Spectroscopic Constants, Vibrational Frequencies, and for the $1\ ^1B_2$ Dipole-Bound Excited State of c-C_3H^-

	EOM-CcCE(TQ)
r_0(C−H) Å	1.081 127
r_0(C−C) Å	1.347 344
$\angle_0$(H−C−C) rad	149.748
r_e(C−H) Å	1.073 426
r_e(C−C) Å	1.370 590
$\angle_e$(H−C−C) rad	150.778
A_e MHz	45 742.38
B_e MHz	35 530.32
C_e MHz	20 006.60
A_0 MHz	45 670.57
B_0 MHz	35 450.27
C_0 MHz	19 969.72
A_1 MHz	45 582.77
B_1 MHz	35 319.21
C_1 MHz	19 908.36
A_2 MHz	45 406.28
B_2 MHz	35 578.63
C_2 MHz	19 899.86
D_J MHz	0.052 317
D_{JK} MHz	-0.157 571
D_K MHz	0.372 654
d_1 MHz	-0.018 459
d_2 MHz	0.001 412
ω_1 cm^{-1} C−H	3384.3
ω_2 cm^{-1} C−C sym. stretch	1634.5
ν_1 cm^{-1}	3120.1
ν_2 cm^{-1}	1534.3
$1\ ^1B_2 \leftarrow \tilde{X}\ ^1A_1$ eV	2.643901
$\tilde{X}\ ^2B_2 \leftarrow \tilde{X}\ ^1A_1$ eV	2.010160
$\tilde{X}\ ^2B_2 \leftarrow 1\ ^1B_2$ eV	-0.633741

the diffuseness of the basis set and related questions as to whether the additional electron is actually bound in the DBXS may have rendered this point moot. A dipole moment of 1.625 D is absolutely required for a dipole-bound state of any kind,[123] but a true state probably requires 2.0 or even 2.5 D.[124] The dipole moment of c-C_3H has been computed to be in this range at $\sim$2.3 D.[114] This radical is cutting it close for possession of a DBXS.

The EOM-CcCE QFF minimum for the $1\ ^1B_2$ DBXS of c-C_3H^- as well as the CcCE QFF minima of the ground states of the anion and neutral radical provide high-level computations for the electron binding energy (eBE) of both anionic states as well as the DBXS transition energy. These are given in Table 2.5. The $1\ ^1B_2 \leftarrow \tilde{X}\ ^1A_1$ transition gives the excitation to the DBXS at 2.644 eV. Unfortunately, the $\tilde{X}\ ^2B_2 \leftarrow \tilde{X}\ ^1A_1$ transition for the eBE of the ground state of the anion is 2.010 eV indicating that the additional electron in the DBXS of c-C_3H^- is likely unbound. Consequently, the hypothesized dipole bound excited state may not be a viable creation mechanism for the formation of the ground state anion in the ISM, casting doubt on the interstellar presence of c-C_3H^- in the first place. However, it has been reported that such adiabatic computations may not provide trustworthy estimates of eBEs due to the fast electronic dynamics present in dipole-bound excitations.[137] Hence, the DBXS of c-C_3H^- may yet be accessible for the creation of the closed-shell anion in the ISM, but the methods utilized here cannot comment in the affirmative to this effect.

Table 2.6: The EOM-CcCE(TQ) 1 $^1B_2$ c-C_3H^- Force Constants (in mdyn/Å^n·rad^m).

F_{11}	6.190 623	F_{111}	-35.1185	F_{332}	-67.4207	F_{1111}	186.27
F_{21}	-0.031 050	F_{211}	2.3777	F_{333}	196.4753	F_{2222}	81.71
F_{22}	9.642 584	F_{221}	-2.5226	F_{551}	-1.5810	F_{3333}	1353.79
F_{31}	0.069 078	F_{222}	-43.7039	F_{552}	6.2892	F_{6633}	705.67
F_{32}	-6.712 843	F_{311}	1.8796	F_{553}	6.7645	F_{6666}	329.28
F_{33}	17.550 721	F_{321}	-0.2747	F_{661}	-2.4117		
F_{55}	0.326 881	F_{322}	18.4377	F_{662}	-11.8345		
F_{66}	0.134 498	F_{331}	0.8044	F_{663}	46.8351		

2.4 Conclusion

$\tilde{X}$ $^2B_2$ c-C_3H is a known and highly-abundant interstellar molecule. It is likely involved in the formation of cyclopropanylidene in the ISM, which, in turn, is likely involved in the formation of interstellar PAHs. While c-C_3H has been observed in the ISM through its rotational transitions and has been deemed even to be more abundant than c-C_3H_2, its vibrational properties have yet to be directly observed.

This work has shown that the three a_1 and one b_1 fundamental vibrational frequencies are all weak absorbers/emitters which is probably one reason as to whey these frequencies have yet to be classified. These four fundamentals have also been provided with the trusted, high-level quantum chemical CcCR QFF VPT2 methodology and should not be greatly affected by the floppy portion of the PES as has been shown previously in other floppy systems.[132,136] These a_1 and b_1 fundamentals for c-C_3H are strongly consistent between quantum chemical methods. Most notably, the CCSD(T)-based CcCR(TQ5) QFF and CCSD-based CcCE(TQ) QFF results are nearly

identical. Furthermore, the CcCR(TQ5) QFF computed rotational constants are in good agreement with experiment giving credence as to the quality of these theoretical spectral determinations. As a result, the ν_1, ν_2, ν_3, and ν_6 fundamental vibrational frequencies of this small, cyclic hydrocarbon are provided for the first time at 3117.7 cm^{-1}, 1564.3 cm^{-1}, 1198.5 cm^{-1}, and 826.7 cm^{-1}, respectively.

However, the two b_2 fundamentals (ν_4 and ν_5) are described poorly by the present approach due to multireference and known, strong pseudo-Jahn-Teller effects that have been explored in this work. The scan of the S_4 C$-$C antisymmetric stretching coordinate reveals that the symmetry-breaking produces a flat PES and potentially even double-well minima making c-C_3H a rather floppy molecule. Most triatomic rings are quite rigid since the triangle is the most stable of structures, but the symmetry-reduced a' labels of the HOMO and HOMO-1 immediately attempt to deform the structure. The quality of single-reference treatment improves, again, after this initial region of C_s symmetry close to the C_{2v} equilibrium point is surpassed. However a Rydberg state crossing within the range of atomic motion (0.350 Å) for vibration may further corrupt future descriptions of this cut on the global c-C_3H PES. Similar behavior is noted in the related DBXS of the c-C_3H^- anion as would be expected for the strong relationships believed to be present between neutrals and corresponding dipole-bound states of anions. In any case, the rotational constants and ν_1 and ν_2 fundamentals have been provided for the $1\ ^1B_2$ DBXS of c-C_3H^- in order to assist in future experimental exploration of this floppy system.

Even though the $1\ ^1B_2$ DBXS of c-C_3H^- struggles to be described in this work due to the related symmetry-breaking in the neutral radical as well as the additional consideration for the

extremely weak or even non-binding of the additional electron, the near-exact behavior between the CcCR QFF and the CcCE QFF for the ground state of the anion as well as that for the neutral radical is promising for the computation of other systems when CCSD(T) is not available. Most notably, CCSD has to be used in the treatment of non-variationally accessible excited states. Hence, the computation of rovibronic properties from EOM-CCSD-based CcCE QFFs beyond that already established[67,86] is quite encouraging.

Chapter 3

Conclusions

While the search for new interstellar molecules continues, quantum chemical methods remain integral for advancement in astrochemical research. The work herein provides strong evidence for the use of quantum theory to characterize and identify new interstellar species and their chemical processes throughout the ISM. Highly accurate QFFs at the CCSD(T) level are used to provide rotational constants and previously undetected anharmonic vibrational modes. Ultimately, the provided data adds to the current knowledge of interstellar chemistry and the creation of PAHs and other primarily carbon molecular species in the interstellar medium.

Bibliography

[1] Morgan, W. J. Quartic Force Fields for Electronically Excited States of Interstellar Medium. M.Sc. thesis, Georgia Southern University, 2015.

[2] Morris, M. *Astrophys. J.* **1975**, *197*, 603–610.

[3] Mauron, N.; Huggins, P. J. *Astron. Astrophys.* **2000**, *359*, 862–885.

[4] Merrill, P. W. *Publ. Astron. Soc. Pacific* **1934**, *46*, 206–207.

[5] Merrill, P. W. *Astrophys. J.* **1936**, *83*, 126–128.

[6] Gratier, P.; Majumdar, L.; Ohishi, M.; Roueff, E.; Loison, J. C.; Hickson, K. M.; Wakelam, V. *The Astrophysical Journal Supplemental Series* **2016**, *225*, 25.

[7] Ohishi, M.; Kaifu, N. *Faraday Disc.* **1998**, *109*, 205–216.

[8] Thaddeus, P.; Vrtilek, J. M.; Gottlieb, C. A. *Astrophys. J.* **1985**, *296*, L63–L66.

[9] Dateo, C. E.; Lee, T. J. *Spectrochim. Acta, Part A.* **1997**, *53*, 1065–1077.

[10] Bakes, E. L.; Tielens, A. G. G. M.; Jr., C. W. B.; Hudgins, D. M.; Aalamandola, L. J. *The Astrophysical Journal* **2001**, *560*, 261–271.

[11] Fortenberry, R. C. *Int. J. Quant. Chem.* **2017**, *117*, 81–91.

[12] Theis, M.; Candian, A.; Tielens, A. G. G. M.; Lee, T. J.; Fortenberry, R. C. *J Phys Chem A* **2015**, 13048–13054.

[13] Planck, M. *Verhandl. Dtsch. phys. Ges.* **1905**, *237*, 2.

[14] Morse, P. M. *Phys. Rev.* **1929**, *33*, 932–947.

[15] Morse, P. M. *Phys. Rev.* **1929**, *34*, 57–64.

[16] Fermi, E.; Serge, E. *Z. Phys. 82*, 729–749.

[17] Herzberg, G. *Atomic Spectra and Atomic Structure*, 2nd ed.; 1937.

[18] Herzberg, G. *Molecular Spectra and Molecules Structure II: Infrared and Raman Spectra of Polyatomic Molecules*, 2nd ed.; Van Nostrand Reinhold, 1945.

[19] Bernath, P. F. *Spectra Atoms and Molecules*, 2nd ed.; Oxford University Press, 2005.

[20] Hollas, J. M. *Modern Spectroscopy*, 4th ed.; Wiley: West Sussex, England, 2004.

[21] Jahn, H. A. *Phys. Rev.* **1939**, *56*, 680–683.

[22] Fermi, E. *Z. Phys.* **1931**, *71*, 250.

[23] Darling, B. T.; Dennison, D. M. *Phys. Rev.* **1940**, *57*, 128–129.

[24] Tarenghi, M. *Astrophys. Space Sci.* **2008**, *313*, 1–7.

[25] Wootten, A.; Thompson, A. R. *Proc. IEEE* **2009**, 1463–1471.

[26] Becklin, E. E.; Gehrz, R. D.; Callis, H. H. S. *Proc. SPIE* **2012**, *8511*.

[27] Becklin, E. E.; Tielens, A. G. G. M.; Gehrz, R. D.; Callis, H. H. S. *Proc. SPIE* **2012**, *6678*, 421–426.

[28] Huang, X.; Lee, T. J. *Astrophys. J.* **2011**, *736*, 33.

[29] Huang, X.; Taylor, P. R.; Lee, T. J. *J. Phys. Chem. A* **2011**, *115*, 5005–5016.

[30] Inostroza, N.; Huang, X.; Lee, T. J. *J. Chem. Phys.* **2011**, *135*, 244310.

[31] Fortenberry, R. C.; Huang, X.; Francisco, J. S.; Crawford, T. D.; Lee, T. J. *J. Chem. Phys.* **2012**, *136*, 234309.

[32] Inostroza, N.; Fortenberry, R. C.; Huang, X.; Lee, T. J. *Astrophys. J.* **2013**, *778*, 160.

[33] Huang, X.; Fortenberry, R. C.; Lee, T. J. *J. Chem. Phys.* **2013**, *139*, 084313.

[34] Fortenberry, R. C.; Huang, X.; Crawford, T. D.; Lee, T. J. *Astrophys. J.* **2013**, *772*, 39.

[35] Zhao, D.; Doney, K. D.; Linnartz, H. *Astrophys. J. Lett.* **2014**, *791*, L28.

[36] Fortenberry, R. C.; Huang, X.; Crawford, T. D.; Lee, T. J. *J. Phys. Chem. A* **2014**, *118*, 7034–7043.

[37] Kitchens, M. J. R.; Fortenberry, R. C. *Chem. Phys.* **2016**, *472*, 119–127.

[38] Schrödinger, E. *Ann. Phys.* **1928**, *79*, 4.

[39] Born, M.; Oppenheimer, J. R. *Ann. Phys.* **1927**, *84*, 457.

[40] Mladenovic, M. *J. Chem. Phys.* **2000**, *112*, 1070–1081.

[41] Hartree, D. R. *Math. Proc. Cambridge* **1927**, *24*, 89–110.

[42] Hartree, D. R. *Math. Proc. Cambridge* **1927**, *24*, 111–132.

[43] Fock, W.; McAllister, T. *Astrophys. J.* **1982**, *257*, L99–L101.

[44] Fischer, C. F. *Comp. Phys. Comm.* **1987**, *43*, 355–365.

[45] Mulliken, R. S. *J Chem Phys* **1955**, *23*, 1833.

[46] Mulliken, R. S. *J Chem Phys* **1955**, *23*, 1841.

[47] Mulliken, R. S. *J Chem Phys* **1955**, *23*, 2338.

[48] Mulliken, R. S. *J Chem Phys* **1955**, *23*, 2343.

[49] Slater, J. C. *Phys. Rev.* **1929**, *34*, 1293.

[50] Scheiner, A. C.; Scuseria, G. E.; Rice, J. E.; Lee, T. J.; Schaefer III, H. F. *J. Chem. Phys.* **1987**, *87*, 5361–5373.

[51] Watts, J. D.; Gauss, J.; Bartlett, R. J. *Chem. Phys. Lett.* **1992**, *200*, 1–7.

[52] Gauss, J.; Stanton, J. F.; Bartlett, R. J. *J. Chem. Phys.* **1991**, *95*, 2623–2638.

[53] Leininger, M. L.; Neilsen, I. M. B.; Crawford, T. D.; Janssen, C. L. *Chem. Phys. Lett.* **2000**, *328*, 431–436.

[54] Gauss, J.; v. R. Schleyer, P. *Wiley* **1990**, *4*, 2574–2578.

[55] Stanton, J. F. *Chem. Phys. Lett.* **1997**, *281*, 130–134.

[56] Lee, T. J.; Scuseria, G. E. In *Quantum Mechanical Electronic Structure Calculations with Chemical Accuracy*; Langhoff, S. R., Ed.; Kluwer Academic Publishers: Dordrecht, 1995; pp 47–108.

[57] Raghavachari, K.; Trucks., G. W.; Pople, J. A.; Head-Gordon, M. *Chem. Phys. Lett.* **1989**, *157*, 479–483.

[58] Crawford, T. D.; Schaefer III, H. F. In *Reviews in Computational Chemistry*; Lipkowitz, K. B., Boyd, D. B., Eds.; Wiley: New York, 2000; Vol. 14; pp 33–136.

[59] Purvis, G. D.; Bartlett, R. J. *J. Chem. Phys.* **1982**, *76*, 1910–1918.

[60] Noga, J.; Bartlett, R. J. *J. Chem. Phys.* **1987**, *86*, 7041–7050.

[61] Scuseria, G. E.; Schaefer III, H. F. *Chem. Phys. Lett.* **1988**, *152*, 382.

[62] Watts, J. D.; Bartlett, R. J. *J. Chem. Phys.* **1990**, *93*, 6104.

[63] Shavitt, I.; Bartlett, R. J. *Many-Body Methods in Chemistry and Physics: MBPT and Coupled-Cluster Theory*; Cambridge University Press: Cambridge, England, 2009.

[64] Watson, J. K. G. In *Vibrational Spectra and Structure*; During, J. R., Ed.; Elsevier: Amsterdam, 1977; pp 1–89.

[65] Fortenberry, R. C.; Huang, X.; Yachmenev, A.; Thiel, W.; Lee, T. J. *Chem. Phys. Lett.* **2013**, *574*, 1–12.

[66] Morgan, W. J.; Fortenberry, R. C. *Spectrochim Acta A Mol Biomol Spectrosc* **2015**, *135*, 965–72.

[67] Morgan, W. J.; Fortenberry, R. C. *J Phys Chem A* **2015**, 7013–7025.

[68] Huang, X.; Lee, T. J. *J. Chem. Phys.* **2008**, *129*, 044312.

[69] Huang, X.; Lee, T. J. *J. Chem. Phys.* **2009**, *131*, 104301.

[70] Fortenberry, R. C.; Huang, X.; Francisco, J. S.; Crawford, T. D.; Lee, T. J. *J. Chem. Phys.* **2011**, *135*, 134301.

[71] Fortenberry, R. C.; Huang, X.; Crawford, T. D.; Lee, T. J. *Astrophys. J.* **2014**, *796*, 139.

[72] Martin, J. M. L.; Lee, T. J. *Chem. Phys. Lett.* **1992**, *200*, 502.

[73] Lee, T. J.; Dateo, C. E. *J. Chem. Phys.* **1997**, *107*, 10373–10380.

[74] Dateo, C. E.; Lee, T. J.; Schwenke, D. W. *J. Chem. Phys.* **1994**, *101*, 5853–5859.

[75] Martin, J. M. L.; Lee, T. J.; Taylor, P. R.; François, J.-P. *J. Chem. Phys.* **1995**, *103*, 2589–2602.

[76] Wheeler, S. E.; Yamaguchi, Y.; Schaefer III, H. F. *J. Chem. Phys.* **2006**, *124*, 044322.

[77] Fortenberry, R. C.; Huang, X.; Francisco, J. S.; Crawford, T. D.; Lee, T. J. *J. Chem. Phys.* **2011**, *135*, 214303.

[78] Fortenberry, R. C.; Huang, X.; Francisco, J. S.; Crawford, T. D.; Lee, T. J. *J. Phys. Chem. A*. **2012**, *116*, 9582–9590.

[79] Helgaker, T.; Ruden, T. A.; Jørgensen, P.; Olsen, J.; Klopper, W. *J. Phys. Org. Chem.* **2004**, *17*, 913–933.

[80] Dunning, T. H. *J. Chem. Phys.* **1989**, *90*, 1007–1023.

[81] Dunning, T. H.; Peterson, K. A.; Wilson, A. K. *J. Chem. Phys.* **2001**, *114*, 9244–9253.

[82] Martin, J. M. L.; Taylor, P. R. *Chem. Phys. Lett.* **1994**, *225*, 473–479.

[83] Kendall, R. A.; Dunning, T. H.; Harrison, R. J. *J. Chem. Phys.* **1992**, *96*, 6796–6806.

[84] M., M. J.; J., L. T. *Chem. Phys. Lett.* **1996**, *258*.

[85] Douglas, M.; Kroll, N. *Ann. Phys.* **1974**, *82*, 89–155.

[86] Morgan, W. J.; Fortenberry, R. C. *Spectrochim. Acta A* **2015**, *135*, 965–972.

[87] Allen, W. D.; coworkers, 2005; $INTDER$ 2005 is a General Program Written by W. D. Allen and Coworkers, which Performs Vibrational Analysis and Higher-Order Non-Linear Transformations.

[88] Mills, I. M. In *Molecular Spectroscopy - Modern Research*; Rao, K. N., Mathews, C. W., Eds.; Academic Press: New York, 1972; pp 115–140.

[89] Papousek, D.; Aliev, M. R. *Molecular Vibration-Rotation Spectra*; Elsevier: Amsterdam, 1982; Vol. 13.

[90] Gaw, J. F.; Willets, A.; Green, W. H.; Handy, N. C. In *Advances in Molecular Vibrations and Collision Dynamics*; Bowman, J. M., Ratner, M. A., Eds.; JAI Press, Inc.: Greenwich, Connecticut, 1991; pp 170–185.

[91] Johnson, C. J.; Poad, B. L. J.; Shen, B. B.; Continetti, R. E. *J. Chem. Phys.* **2011**, *134*, 171106.

[92] Johnson, C. J.; Harding, M. E.; Poad, B. L. J.; Stanton, J. F.; Continetti, R. E. *J. Am. Chem. Soc.* **2011**, *133*, 19606–19609.

[93] Turney, J. M. et al. *Wiley Interdisciplinary Reviews: Computational Molecular Science* **2012**, *2*, 556–565.

[94] Werner, H.-J. et al. MOLPRO, version 2010.1, a Package of $Ab\ Initio$ Programs. 2010; see http://www.molpro.net.

[95] Savage, B. D.; Sembach, K. R. *Annu. Rev. Astron. Astrophys.* **1996**, *34*, 279–329.

[96] Cardelli, J. A.; Meyer, D. M.; Jura, M.; Savage, B. D. *Astrophys. J.* **1996**, *467*, 334–340.

[97] Clary, D. C.; Buonomo, E.; Sims, I. R.; Smith, I. W. M.; Geppert, W. D.; Naulin, C.; Costes, M.; Cartechini, L.; Casavecchia, P. *J Phys Chem A* **2002**, *106*, 5541–5552.

[98] McCarthy, M. C.; Thaddeus, P. *J Chem Phys* **2005**, *122*, 174308.

[99] Tucker, K. D.; Kutner, M. L.; Thaddeus, P. *Astrophys. J.* **1974**, *193*, L115–L119.

[100] Guélin, M.; Green, S.; Thaddeus, P. *The American Astronomical Society* **1978**, *224*, L27–L30.

[101] Cernicharo, J.; Kahane, C.; Gómez-González, J.; M.Guélin, *Astron. Astrophys.* **1986**, *164*, L1–L4.

[102] Cernicharo, J.; Kahane, C.; Gómez-González, J.; M.Guélin, *Astron. Astrophys.* **1986**, *167*, L5–L7.

[103] Cernicharo, J.; Guélin, M.; Walmsley, C. M. *Astron. Astrophys.* **1987**, *172*, L5–L6.

[104] Suzuki, H.; Ohishi, M.; Kaifu, N.; Ishikawa, S.; Kasuga, T.; Saito, S.; Kawaguchi, K. *Publ. Astron. Soc. Japan* **1986**, *38*, 911–917.

[105] Guélin, M.; Cernicharo, J.; Kahane, C.; Gómez-González, J.; Walmsley, C. M. *Astron. Astrophys.* **1987**, *175*, L5–L8.

[106] Guelin, M.; Cernicharo, J.; McCarthy, M. C.; Gottlieb, C. A.; Thaddeus, P.; Ohishi, M.; Saito, S.; Yamamoto, S. *Astron. Astrophys.* **1997**, *317*, L1–L4.

[107] Gottlieb, C. A.; Vrtilek, J. M.; Gottlieb, E. W.; Thaddeus, P.; Hjalmarson, A. *Astrophys. J.* **1985**, *294*, L55–L58.

[108] Yamamoto, S.; Saito, S. *J Chem Phys* **1994**, *101*, 5484–5493.

[109] Xie, H. B.; Ding, Y. H.; Sun, C. C. *J Comput Chem* **2006**, *27*, 641–660.

[110] Kaiser, R. I.; Ochsenfeld, C.; Head-Gordon, M.; Lee, Y. T.; Suits, A. G. *Science* **1996**, *274*, 1508–1510.

[111] Thaddeus, P.; Gottlieb, C. A.; Hjalmarson, A.; Johansson, L. E. B.; Irvine, W. M.; Friberg, P.; Linke, R. A. *Astrophys. J.* **1985**, *294*, L49–L53.

[112] Yamamoto, S.; Saito, S.; Guèlin, M.; Cernicharo, J.; Suzuki, H.; Ohishi, M. *Astrophys. J.* **1987**, *322*, L55–L58.

[113] Aoki, K.; Ikuta, S.; Murakami, A. *Theor. Chem. Acc.* **1996**, *365*, 103–110.

[114] Stanton, J. F. *Chem. Phys. Lett.* **1995**, 20–26.

[115] Jiang, Q.; Rittby, C. M. L.; Graham, W. R. M. *J Chem Phys* **1993**, *99*, 3194–3199.

[116] Halvick, P. *Chem. Phys.* **2007**, *340*, 79–84.

[117] Yamagishi, H.; Taiko, H.; Shimogawara, S.; Murakami, A.; Noro, T.; Tanaka, K. *Chem. Phys. Lett.* **1996**, *250*, 165–170.

[118] Sheehan, S. M.; Parsons, B. F.; Zhou, J.; Garand, E.; Yen, T. A.; Moore, D. T.; Neumark, D. M. *J Chem Phys* **2008**, *128*, 034301(1)–034301(13).

[119] Fortenberry, R. C.; Thackston, R. *Int. J. Quant. Chem.* **2015**, $in\ press$.

[120] Pino, T.; Tulej, M.; Güthe, F.; Pachkov, M.; Maier, J. P. *J. Chem. Phys.* **2002**, *116*, 6126–6131.

[121] Agúndez, M.; Cernicharo, J.; Guélin, M.; Gerin, M.; McCarthy, M. C.; Thaddeus, P. *Astron. Astrophys.* **2008**, *478*, L19–L22.

[122] Carelli, F.; Gianturco, F. A.; Wester, R.; Satta, M. *J. Chem. Phys.* **2014**, *141*, 054302.

[123] Fermi, E.; Teller, E. *Phys. Rev.* **1947**, *72*, 399–408.

[124] Gutsev, G.; Adamowicz, A. *Chem. Phys. Lett.* **1995**, *235*, 377–381.

[125] Morgan, W. J.; Fortenberry, R. C. *J. Phys. Chem. A* **2015**, *119*, 7013–7025.

[126] Fortenberry, R. C.; Crawford, T. D.; Lee, T. J. *J. Phys. Chem. A*. **2013**, *117*, 11339–11345.

[127] Christiansen, O.; Koch, H.; Jørgensen, P. *J. Chem. Phys.* **1995**, *103*, 7429–7441.

[128] Koch, H.; Christiansen, O.; Jørgensen, P.; de Meràs, A. M. S.; Helgaker, T. *J. Chem. Phys.* **1997**, *106*, 1808–1818.

[129] Smith, C. E.; King, R. A.; Crawford, T. D. *J. Chem. Phys.* **2005**, *122*, 054110–1–8.

[130] Lee, T. J.; Taylor, P. R. *Int. J. Quant. Chem.* **1989**, *36*, 199–207.

[131] Fortenberry, R. C.; King, R. A.; Stanton, J. F.; Crawford, T. D. *J. Chem. Phys.* **2010**, *132*, 144303.

[132] Yu, Q.; Bowman, J. M.; Fortenberry, R. C.; Mancini, J. S.; Lee, T. J.; Crawford, T. D.; Klemperer, W.; Francisco, J. S. *J Phys Chem A* **2015**, *119*, 11623–11631.

[133] Møller, C.; Plesset, M. S. *Phys. Rev.* **1934**, *46*, 618–622.

[134] Hehre, W. J.; Ditchfeld, R.; Pople, J. A. *J. Chem. Phys.* **1972**, *56*, 2257.

[135] Frisch, M. J. et al. Gaussian 09 Revision D.01. Gaussian Inc. Wallingford CT 2009.

[136] Fortenberry, R. C.; Yu, Q.; Mancini, J. S.; Bowman, J. M.; Lee, T. J.; Crawford, T. D.; Klemperer, W. F.; Francisco, J. S. *J Chem Phys* **2015**, *143*.

[137] Simons, J. *J. Phys. Chem. A.* **2008**, *112*, 6401–6511.